AD-A263 495

WL-TR-92-2086

PULSE MITIGATION AND HEAT TRANSFER ENHANCEMENT TECHNIQUES

VOL 1 - SPRAY COOLING

L. C. Chow
D. E. Tilton
M. R. Pais

University of Kentucky
Department of Mechanical Engineering
Lexington, KY 40506-0046

AUG 1992

FINAL REPORT FOR 07/01/87 - 07/31/92

APPROVED FOR PUBLIC RELEASE; DISTRIBUTION IS UNLIMITED

AERO PROPULSION AND POWER DIRECTORATE
WRIGHT LABORATORY
AIR FORCE MATERIEL COMMAND
WRIGHT-PATTERSON AFB OH 45433-6563

NOTICE

When Government drawings, specifications, or other data are used for any purpose other than in connection with a definitely Government-related procurement, the United States Government incurs no responsibility or any obligation whatsoever. The fact that the government may have formulated or in any way supplied the said drawings, specifications, or other data, is not to be regarded by implication, or otherwise in any manner construed, as licensing the holder, or any other person or corporation; or as conveying any rights or permission to manufacture, use, or sell any patented invention that may in any way be related thereto.

This report is releasable to the National Technical Information Service (NTIS). At NTIS, it will be available to the general public, including foreign nations.

This technical report has been reviewed and is approved for publication.

Michael J Morgan
MICHAEL J. MORGAN
Project Engineer

Jerry E Beam
JERRY E. BEAM, Chief
Thermal Technology Section

Michael D Braydich
MICHAEL D. BRAYDICH, Lt Col, USAF
Deputy Chief
Aerospace Power Division
Aero Propulsion & Power Directorate

If your address has changed, if you wish to be removed from our mailing list, or if the addressee is no longer employed by your organization please notify WL/POOS, WPAFB, OH 45433-6563 to help us maintain a current mailing list.

Copies of this report should not be returned unless return is required by security considerations, contractual obligations, or notice on a specific document.

WL-TR-92-2086

PULSE MITIGATION AND HEAT TRANSFER ENHANCEMENT TECHNIQUES

VOL 1 - SPRAY COOLING

L. C. Chow
D. E. Tilton
M. R. Pais

University of Kentucky
Department of Mechanical Engineering
Lexington, KY 40506-0046

AUG 1992

FINAL REPORT FOR 07/01/87 - 07/31/92

APPROVED FOR PUBLIC RELEASE; DISTRIBUTION IS UNLIMITED

AERO PROPULSION AND POWER DIRECTORATE
WRIGHT LABORATORY
AIR FORCE MATERIEL COMMAND
WRIGHT-PATTERSON AFB OH 45433-6563

NOTICE

When Government drawings, specifications, or other data are used for any purpose other than in connection with a definitely Government-related procurement, the United States Government incurs no responsibility or any obligation whatsoever. The fact that the government may have formulated or in any way supplied the said drawings, specifications, or other data, is not to be regarded by implication, or otherwise in any manner construed, as licensing the holder, or any other person or corporation; or as conveying any rights or permission to manufacture, use, or sell any patented invention that may in any way be related thereto.

This report is releasable to the National Technical Information Service (NTIS). At NTIS, it will be available to the general public, including foreign nations.

This technical report has been reviewed and is approved for publication.

Michael J. Morgan
MICHAEL J. MORGAN
Project Engineer

Jerry E. Beam
JERRY E. BEAM, Chief
Thermal Technology Section

Michael D. Braydich
MICHAEL D. BRAYDICH, Lt Col, USAF
Deputy Chief
Aerospace Power Division
Aero Propulsion & Power Directorate

If your address has changed, if you wish to be removed from our mailing list, or if the addressee is no longer employed by your organization please notify WL/POOS, WPAFB, OH 45433-6563 to help us maintain a current mailing list.

Copies of this report should not be returned unless return is required by security considerations, contractual obligations, or notice on a specific document.

REPORT DOCUMENTATION PAGE

Form Approved
OMB No. 0704-0188

1. AGENCY USE ONLY (Leave blank)	2. REPORT DATE	3. REPORT TYPE AND DATES COVERED
	AUG 1992	FINAL 07/01/87 - 07/01/92

4. TITLE AND SUBTITLE
PULSE MITIGATION AND HEAT TRANSFER ENHANCEMENT TECHNIQUES
VOL. 1 - SPRAY COOLING

5. FUNDING NUMBERS
C: F33615-87-C-2777
PE 63218
PR D812
TA 00
WU 08

6. AUTHOR(S)
L. C. CHOW
D. E. TILTON
M. R. PAIS

7. PERFORMING ORGANIZATION NAME(S) AND ADDRESS(ES)
University of Kentucky
Department of Mechanical Engineering
Lexington, KY 40506-0046

8. PERFORMING ORGANIZATION REPORT NUMBER
UK-ME-92-02

9. SPONSORING/MONITORING AGENCY NAME(S) AND ADDRESS(ES)
MICHEAL MORGAN (513/255-2922)
AERO PROPULSION AND POWER DIRECTORATE (WL/POOS)
WRIGHT LABORATORY
WRIGHT-PATTERSON AIR FORCE BASE, OHIO 45433-6563

10. SPONSORING/MONITORING AGENCY REPORT NUMBER
WL-TR-92-2086

11. SUPPLEMENTARY NOTES

12a. DISTRIBUTION/AVAILABILITY STATEMENT
APPROVED FOR PUBLIC RELEASE; DISTRIBUTION IS UNLIMITED.

12b. DISTRIBUTION CODE

13. ABSTRACT (Maximum 200 words)

This report presents an experimental and theoretical investigation of spray cooling. A complete study is presented for surfaces maintained between the fluid saturation temperature and the Leidenfrost temperature. Experiments were conducted to analyze the effects of spray and surface conditions on the heat transfer. Different mechanisms causing the critical heat flux (CHF)are identified. For dropwise evaporation, CHF results when the surface heat flux exceeds the latent heat content of the spray. As the flow rate is increased, droplet conglomeration and surface flooding result. For low flow rate cases with a flooded surface, CHF is caused by a liquid deficiency resulting from droplet expulsion caused by the nucleating bubbles within the liquid film. For higher flow rate cases, CHF occurs when the vapor generation rate on the surface is so high that a vapor barrier is formed.

14. SUBJECT TERMS
EVAPORATIVE COOLING, SPRAY COOLING, HIGH HEAT FLUX, MAXIMUM HEAT FLUX, DROPLET IMPINGEMENT

15. NUMBER OF PAGES
138

16. PRICE CODE

17. SECURITY CLASSIFICATION OF REPORT	18. SECURITY CLASSIFICATION OF THIS PAGE	19. SECURITY CLASSIFICATION OF ABSTRACT	20. LIMITATION OF ABSTRACT
UNCLASSIFIED	UNCLASSIFIED	UNCLASSIFIED	UL

i

Table of Contents

List of Figures

List of Tables

Nomenclature

C_p	Specific heat at constant pressure J/kg·K
F	Free energy J
k	Thermal conductivity W/m·K
p	Pressure N/m^2
q	Heat flux W/cm^2
r	Radius m
T	Temperature °C
V	Voltage V

Greek

λ	Roughness spacing
Γ	Latent heat of vaporization J/kg
σ	Surface tension N/m
ν	Specific volume m^3/kg
ϕ	Angle of contact on vapor side
θ	Contact angle

Subscripts

ag	Silver
b	Bubble
cn	Constantan
cu	Copper
lg	Liquid gas interface
liq	Liquid
m	Minimum

sat Saturation

w Wall

Superscript

" Vapor phase

Chapter 1

Introduction

The rapid advances made in electronic technology have long since overtaken the developments in heat transfer with the result that removal of heat has become the major impediment in the path of further developments in miniaturization of electronic chips. As the size of the electronic chip decreases the number of components per unit area increases with the result that the heat generated per unit area also increases. This necessitates the use of more efficient methods of heat removal than those in use earlier. Also it is desirable to maintain the temperature of the chip within a small temperature range while the dissipation of heat varies according to the requirements from the chip. The requirements stated above are beyond the capability of currently used cooling techniques.

Many other applications in advanced aircraft and spacecraft systems which require the development of an efficient cooling technique are also arising. The sensitive components in these systems must be maintained at a low temperature to operate reliably; also the heat must be rejected to the ambient. In the case of spacecraft systems, this heat must be rejected by radiation. For a given heat load, the radiator area is inversely proportional to the fourth power of the heat rejection temperature. Since a high efficiency heat removal allows a high heat rejection temperature, the radiator area may be reduced

considerably. Similarly for advanced aircraft applications a very efficient heat transfer allows minimization in size and weight of the heat transfer components. These factors are very important in aircraft and spacecraft design since reduced size and weight mean improved performance and cost reductions.

All this has led to the interest being focused on heat transfer enhancement involving phase change processes. Such processes take advantage of the fact that a pure substance will absorb or release a substantial quantity of heat at a fixed temperature during its phase change process. The exchange of this latent heat is feasible at a low temperature difference between the heat transfer surface and the phase change material, and depending on the conditions, the magnitude can be far greater than the corresponding sensible heat exchange for the same temperature difference.

Spray cooling [1-4] which involves spraying the hot surface with an atomized liquid, in particular, has proved to be far more efficient than the conventional pool boiling method of heat removal [5-8]. The phase change process in spray cooling is controlled by convection, conduction and nucleation.

Spray cooling can be divided into two categories depending on the mode of atomizing the liquid. The spray can be produced by either a pressure atomizing nozzle [1-3] or a gas atomizing nozzle [4]; the latter has been shown to have better heat transfer characteristics. Both modes can be further categorized into two regimes based on the droplet density (i.e., the number of droplets per unit volume of the spray close to the heat

transfer surface). The dilute spray regime involves very low droplet densities with the result that the droplets falling on the surface do not interfere with one another. Due to their momentum, the droplets form thin discs of liquid on impacting the surface; these discs then evaporate by absorbing heat from the surface. The number of droplets falling on the surface is such that these discs do not interfere with one another. As is obvious the rate of evaporation of these discs and the frequency of the spray droplets will determine whether the discs will interact or not. Hence, the characterization of the spray depends on the temperature of the surface, a spray which is dilute at a high temperature may not be considered dilute at a lower temperature.

The other spray regime involves dense spray, i.e., the number of droplets impinging on the heated surface is so large that there is extensive interaction between individual droplets upon reaching the surface. As explained earlier each droplet forms a thin disc of liquid upon impinging on the surface; if the number of droplets is large, the droplets impinging close to each other will affect each other such that the liquid from these droplets will merge to form a thin film of liquid on the surface. If the rate of evaporation of this liquid film is lesser than the rate of incoming liquid, the subsequent droplets will impinge on a thin liquid film instead of the heat transfer surface. If the spray is produced by a gas atomized nozzle, the gas flow will form a stagnation flow field on the surface of the film and hence squeeze the film. Thus, the impinging droplets

will maintain a liquid film on the surface, the thickness of this film depending on the influx of liquid, the rate of evaporation, the surface conditions and the atomizing gas flow rate(in the case of gas atomized spray).

The dilute regime of spray cooling has been investigated in detail by Bonacina et al.[9] and the mechanism for heat transfer has been fairly well established. The dilute regime of spray cooling is characterized by very efficient heat transfer due to the evaporation of liquid droplets falling on the heated surface. As explained earlier the liquid droplets upon falling on the surface form thin discs of liquid, the thickness of the each disc depending on the velocity of the impinging droplet and its diameter, the liquid at the free surface of these discs then evaporates by heat conducted through the liquid from the heat transfer surface. The low liquid flow rates involved in this regime limit its heat removal capacity and thereby its applications. Hence, this study deals only with the dense spray regime of gas atomized spray cooling system.

As with any other new technique most of the early research in spray cooling involved experimental studies. One of the earliest studies was done by Toda [10], heat fluxes of over 250 W/cm^2 at surface superheats of 30-60 °C were reported in the study. A very simplistic model which did not take convection and nucleation into account was also proposed, the model assumed that conduction through the liquid film is the only contributing phenomenon leading to the evaporation from the free surface. Eastman and Ernst [11] reported heat fluxes of upto 2000 W/cm^2

at surface temperatures of about 300 °C. Pais et al. [4] investigated spray cooling with air atomizing nozzles and reported heat fluxes over 1000 W/cm² at a surface temperature as low as 105 °C. They studied the effect of surface roughness and showed that a very smooth surface is extremely efficient for heat transfer in this mode of spray cooling. This effect was also observed during the course of the present study and is described in detail in Chapter 4. Tilton [12] studied spray cooling using a pressure atomizing nozzle in a closed system and reported a maximum heat flux of around 800 W/cm² at a surface temperature of about 130 °C, an attempt was also made to explain the CHF (critical heat flux) phenomena in spray cooling. A phase Doppler particle analyzer (PDPA) was used to measure the diameter and velocity of the droplets impinging on a hot surface. It was observed that near CHF a large fraction of the liquid impinging on the surface is thrown back in the form of droplets from the liquid film due to expulsion caused by 1) vapor bubbles bursting in the film and, 2) by splashing. Due to this expulsion there is an upper limit on the heat flux for a particular spray condition, this heat flux being the critical heat flux.

No comprehensive model has so far been proposed to explain all the phenomena involved in spray cooling due to the very complex nature of the process. From the results of previous research it is seen that spray characteristics like droplet size, droplet density and droplet velocity play an important part in determining the spray cooling heat transfer. In order

to obtain a better understanding of the spray cooling process this study investigates the effect of various parameters, e.g., liquid flow rate, liquid temperature and atomizing gas (air in this case) flow rate, on spray cooling characteristics. The chief focus of this study, however, is on the effect of the heat transfer surface characteristics, i.e., surface roughness and wettability. To this effect, experiments were conducted using various spray configurations on surfaces with different surface characteristics.

The following chapters present the theory of spray cooling, the description of the experimental set-up and procedure and finally the results and conclusions.

Chapter 2
Theory of Spray Cooling

2.1 Pool Boiling

A knowledge of pool boiling is essential in understanding the phenomena involved in spray cooling heat transfer. Figure 2.1 shows the pool boiling curve for water [13], the heat flux observed during pool boiling conditions is plotted versus the temperature of the heat transfer surface. As seen from the plot the heat transfer process can be divided into three regimes. The first, known as the Nucleate boiling regime, is characterized by formation of vapor bubbles at nucleation sites on the surface; an increase in temperature causes increased nucleation resulting in increased phase change. As shown in Figure 2.1 the nucleate boiling portion of the curve has a very steep slope, indicating a high heat transfer coefficient.

This region starts from the point when bubbles are first observed to form; this is known as the onset of nucleate boiling (ONB). As shown on the plot, ONB occurs at a temperature higher than 100 °C because the mechanical and thermal equilibrium requirements do not permit a vapor bubble to exist and grow at a lower temperature. For mechanical equilibrium a bubble must satisfy the following requirement:

$$(p_{sat}(T_b) - p_{liq})\cdot\pi\cdot r^2 = 2\cdot\pi\cdot r\cdot\sigma$$

$$\text{or:} \quad p_{sat}(T_b) = \frac{2\cdot\sigma}{r} + p_{liq} \qquad (2.1)$$

It follows from eqn. 2.1 that the pressure of the saturated vapor inside a bubble must be greater than the pressure of the surrounding liquid. For thermal equilibrium the temperature of the vapor inside the bubble (T_b) must be equal to the temperature of the surrounding liquid, if the surrounding liquid is hotter the liquid will evaporate into the bubble increasing its size and if the liquid is cooler the vapor inside will condense into the liquid till equilibrium is reached. Thus, to satisfy both these conditions the liquid temperature should be such that the pressure of the saturated vapor at this temperature be sufficient to balance the surface tension forces and the external pressure as shown in eqn. 2.1. This requirement can only be satisfied if the liquid is superheated (i.e., its temperature is higher than the saturation temperature corresponding to the liquid pressure), thus, the surface temperature for ONB is higher than 100 °C.

As the surface temperature increases, more and more bubbles are formed; a point is reached when the frequency of bubbles ejected becomes so high that a column of vapor is formed above the nucleation site; this is also known as jet boiling. Hydrodynamic instabilities cause these vapor columns to merge at some positions to from vapor blankets on the heated surface; if the surface temperature is maintained constant, these vapor

blankets alternate with the jet boiling; the vapor blankets allow very low heat transfer from the surface and hence go towards reducing the heat flux. The point where the heat flux begins decreasing with increasing temperature is known as the critical heat flux (CHF). If temperature is increased further, the heat flux continues to decrease till a point is reached when the vapor blanket exists between the liquid and the heat transfer surface continuously; this temperature shown on the curve is the Leidenfrost temperature. The region between the CHF point and the Leidenfrost temperature is known as transition boiling.

After the Leidenfrost temperature, the heat transfer takes place between the hot surface and the liquid above it through the vapor film. The heat is transferred through the film by natural convection and, hence, an increase in surface temperature beyond Leidenfrost point results in an increase in heat flux. This regime of boiling is known as the film boiling regime. The various stages of the pool boiling curve are shown in Figure 2.2 [13].

Nucleate boiling is the preferred mode for most practical applications of pool boiling heat transfer since it involves relatively low temperatures and results in significant heat transfer. It should be noted that the heat flux is the independent parameter in most cases, i.e., the heat flux and not the temperature is controlled directly. In such cases the transition boiling regime cannot be realized; when the heat flux increases slightly above the CHF, there occurs a temperature

overshoot because the mode of boiling changes from nucleate boiling to film boiling. As shown in the curve the temperature on the film boiling region of the curve corresponding to the critical heat flux is quite high and in most cases such a high temperature cannot be tolerated. The main limitation of pool boiling is, thus, the fact that the maximum heat flux from the surface should be below the CHF. This condition is not suitable for many applications which require heat fluxes higher than the CHF at temperatures below the Leidenfrost temperature.

2.2 Spray Cooling

As mentioned in the introduction, spray cooling [1-4] has been shown to be capable of handling much higher heat fluxes at temperatures much lower than the Leidenfrost temperature. Figure 2.3 illustrates the physics of evaporation/boiling taking place within a thin film of liquid deposited on a hot surface by droplet impingement assisted by an external gas stagnation flow field. If the film is ultra-thin (of the order of a few microns in the case of water), then the heat can be conducted through the liquid to the surface, where the liquid will evaporate directly into the ambient (note that the effective conductivity of the liquid is increased due to the convection caused by impinging droplets). An air/droplet impingement field on the surface due to an air atomizing nozzle is shown in Figure 2.3. The air jet on impinging the surface forms a stagnation point flow field. The drops do not follow the air streamlines close to the surface due to their relatively higher inertia. These

drops impinge on the hot surface to form flat discs, whose thickness is much lower than the diameter of the drop [14]. Simultaneously, the stagnation flow field spreads the droplets/discs further, through shear forces, to form a thin film on the surface. The number of droplets falling on the surface being very large, these thin discs interact to form a uniform thickness film on the surface. The large number of droplets impinging on the liquid film cause a turbulent flow field inside the film; this results in very intense mixing of the liquid and thereby leads to greatly increased convection heat transfer. This mixing causes the hot liquid in contact with the surface to be displaced to the free surface where it evaporates. Such a process essentially increases the effective thermal conductivity of the film. The free surface of the liquid film has to be in thermodynamic equilibrium with the vapor in its immediate vicinity; therefore, the temperature of the free surface is equal to the saturation temperature corresponding to the partial vapor pressure over the free surface of the film. The whole mixing process can thus be viewed as enhanced conduction heat transfer through the liquid film with the temperature drop across the liquid film being equal to :

$$\Delta T = T_{surface} - T_{sat} \qquad (2.2)$$

where T_{sat} refers to the saturation temperature corresponding to the partial vapor pressure near the free surface of the film and $T_{surface}$ refers to the temperature of the heat transfer surface.

The vapor emanating due to evaporation is swept away by the stagnation air flow field, hence, the effect of the stagnation flow field is to reduce the partial vapor pressure in the vicinity of the liquid film surface by clearing away the evolving vapor. This reduction in partial vapor pressure near the free surface of the film causes a reduction in the liquid temperature required for evaporation (saturation temperature). This effect is shown in Figure 2.4; the plot of partial vapor pressure versus the saturation temperature. Therefore, the net effect of the stagnation air flow field is to squeeze the liquid film and enhance evaporation by reducing the saturation temperature on the free surface of the liquid film. Thus, the possibility of phase change below 100°C, i.e., with negative superheats, exists for water at 1-atm ambient pressure.

Concurrently, if the superheat is sufficient, nucleation will occur at the liquid-solid interface, the radius above which the bubble will survive and grow being given by [15] :

$$r_m'' = \frac{2\sigma\nu'' T_s}{\Gamma(T_w - T_s)} \qquad (2.3)$$

2.3 <u>Surface Roughness Effects</u>

In the case of nucleate boiling, roughness plays a governing role in the enhancement of heat transfer. The cavities created by the roughness serve as regions of vapor germination and entrapment. When a growing bubble reaches the point where the buoyancy forces overcome the surface tension forces holding it to the surface, the bubble departs from the

surface and liquid flows in to take the place formerly occupied by the vapor. As shown in Figure 2.5, the geometry of the cavity and wettability of the surface determine whether any vapor will be trapped in the cavity [16]. If the trapped vapor bubble has a large radius of curvature, then the degree of superheat required for nucleation reduces (eqn. 2.3). This enhances heat removal (because of phase change) along with maintaining a constant surface temperature near saturation condition, the degree of superheat being a function of roughness spacing [17]. The roughness spacing determines the cavity size for vapor/gas entrapment, consequently the amount of nucleation taking place at a particular temperature depends on the roughness. Secondly the heat transfer also improves due to the increase in surface area subtended by the roughness elements. Referring to Figure 2.6, the smaller elements act as nucleating sites, and provide a sizeable increase in area, as compared to the larger undulations of the overall surface, over which the smaller elements are distributed.

The heat transfer and the nucleation site density depend on the distribution of the roughness elements, i.e., primarily on λ, the spacing between the roughness elements [8,18]. Consider nucleation on a rough wall, as the density of the nucleation sites increases, at first the heat flux will increase as would be expected. However, as the nucleation sites get closer, the growth of the bubbles created by adjacent sites will cause the bubbles to combine and form a vapor barrier leading to dryout [19-21]. Hence, there may exist a configuration which produces

the maximum heat flux at the lowest superheat, the spacing in this configuration, being far more than that for a densely packed surface [22].

When a bubble forms, a thin microlayer of liquid which lies just between the vapor and the hot surface governs the rate of evaporation into the bubble, and in the case of water, takes between 50 μs to 2 ms to disappear [23,24]. As shown in Figure 2.7, the bubble grows further by evaporation through its walls, heat being conducted from the hot surface through the surrounding liquid. This latter process is much slower than the direct evaporation of the microlayer. Consequently, the heat removal can be further enhanced if the microlayer can be continuously maintained. This can be realized if the bubble is removed the instant its microlayer evaporates, making available that site for a new bubble to form on a fresh microlayer [21].

In spray cooling, the thermal boundary layer is limited by the thickness of the liquid film. The bubble on emerging from the cavity and growing in the liquid film will be exposed to temperature gradients and the forces of the external flow field. The bubble temperature being higher, will induce the walls to evaporate into the ambient. Secondly, the temperature gradients will make it unstable [25,26]. Thirdly, the external droplet/ambient flow field also assists in the early departure/breakup of the bubble. Thus, the bubble breaks up much before it would in pool boiling or even in most cases of flow boiling, thus enabling a higher heat flux to exist at a

lower superheats.

Another phenomenon which comes into play in spray cooling process is the secondary nucleation phenomenon [27]. As shown in Figure 2.8, when a droplet of liquid hits a liquid surface small bubbles of gas/vapor are trapped by the liquid because of the disturbance caused on the surface; these gas/vapor bubbles have a lower partial vapor pressure than a bubble which originates in the liquid. Due to this, the high temperature liquid surrounding these bubbles will evaporate into them to maintain thermal equilibrium; this evaporation enhances the phase change heat transfer. This enhancement of phase change heat transfer due to the bubbles entrained by the impinging droplets on a liquid surface is known as secondary nucleation [27]. The impinging spray droplets, thus, enhance phase change process further by secondary nucleation phenomenon.

2.4 Surface Wettability Effects

The phenomenon of wettability, which can be ascribed to the surface tension forces at the liquid/solid interface, plays a controlling part in nucleation and boiling [28-31]. The effect of contact angle is most pronounced at CHF in pool boiling, a lower contact angle provides better wetting and thus delays the formation of the vapor blanket leading to a higher transition heat flux [29-31]. The effect of contact angle on spray cooling has not been studied earlier and this is one of the purposes of this study.

Referring to Figure 2.9, the free energy of formation ΔF of a vapor nucleus of radius r_{lg}, for a contact angle $\theta = \pi - \phi$, and surface tension σ_{lg}, can be written as [15] :

$$\Delta F = \frac{2}{3} \sigma_{lg} \pi r_{lg}^2 (1 - \cos\phi - \frac{1}{2}\cos\phi \sin^2\phi)$$

Hence, for $\phi \to 0$ the value of the free energy change $\Delta F \to 0$, and for $\phi = \pi$, $\Delta F = \Delta F_{sphere}$. This implies that a vapor bubble will first form on a solid surface (heterogeneous nucleation) rather than within the liquid (homogeneous nucleation). A deduction of the above analysis indicates that since :

$$\phi = \pi - \theta$$

the contact angle must be π (i.e., $\phi = 0$) for maximizing vapor nucleus generation. However, this would create a vapor film on the surface which would drastically reduce heat transfer. Also the liquid would not wet the surface, thus creating hot spot regions leading to dryout. If the contact angle $\theta \to 0$, i.e., the liquid wets the surface completely, then $\phi \to \pi$; this demands the maximum change in free energy for nucleation. This is because, for a hypothetical perfectly wetting liquid, the bubble is forced to form in the homogeneous liquid or is ejected off the solid surface into the liquid medium by the advancing liquid. In wetting the whole surface, the liquid provides maximum contact between the coolant and the heat dissipating surface. If evaporation from the free surface of the liquid is the dominating heat transfer mechanism, then the suppression of nucleation will be advantageous because no resistance to heat

transfer will arise due to the formation of a vapor barrier between the liquid and the hot surface. However, if the conduction resistance from the hot surface through the liquid to the free surface is large, then the nucleation phenomenon will play the controlling role. In such a case, a perfectly wetting liquid provides maximum liquid/solid contact but is not conducive to nucleation. On the other hand, a nonwetting liquid, even though optimum for nucleation, does not provide sufficient liquid/solid contact, thus leading to dryout. Referring to Figure 2.5, for rough surfaces entrapment of gas/vapor within the cavity is determined by [16] :

$$\theta > \text{included angle formed by the cavity walls}$$

All this implies that a perfectly wetting liquid is not advantageous for the nucleation process though it may be better near the dryout region.

In spray cooling variations in contact angle θ can be achieved by selecting different liquid/solid combinations, and by spraying the liquid using a gas atomizing nozzle, the following can be achieved:

a) The liquid is spread over the surface as a flat film (due to the secondary stagnation flow of the gas) even though $\theta > 0$, thus maximizing liquid/solid contact for heat transfer.

b) The flat film with the reduced vapor pressure at the free surface (due to the secondary stagnation flow field of the gas which sweeps away the vapor produced) provides optimum conditions for evaporation at the liquid /ambient interface.

With reference to Figure 2.3, the air jet impingement on the surface squeezes the impinging liquid droplets into a very thin film, sweeping off the excess liquid and any evolving vapor. Hence, wettability is enhanced for liquid/solid combinations which do not have contact angles near zero.

The effect of the above surface parameters, i.e., roughness, and wettability, on the heat transfer characteristics of spray cooling was examined experimentally and the details are presented in the following chapters.

Chapter 3

Experiments

3.1 Heater Block Design

Due to the large temperature gradients required to drive large heat fluxes through any surface, care must be taken in the design of the apparatus so as to arrive at temperatures within the body which maintain the physical and chemical integrity of the system.

Referring to Figure 3.1, a lightweight heater of cylindrical construction using three miniature quartz radiation lamps (capable of providing a total of about 1,050 W) was designed and fabricated so as to provide a low thermal mass permitting finer control and measurement of the thermal behavior during the boiling/evaporation process. The quartz radiation lamps consist of a quartz bulb containing a tungsten coil which is heated by electrical current. The temperature of the coil reaches a temperature of approximately 3000 K at the maximum rated voltage. The lamps are housed in the copper block such that most of the radiation from the lamps is absorbed by the block.

The heater block as shown in Figure 3.1 is of laminate copper-constantan construction which provides the ability to measure surface temperature and determine the heat flux. The laminate copper-constantan integral thermocouples in effect provide an accurate temperature measurement across the

constantan strip which in turn allows a precise prediction of surface temperature and heat flux.

The very low thermal conductivity of constantan enables a large temperature drop across its thickness. The heat flux and the surface temperature extrapolation depend on the thickness of the constantan film, a thicker film will reduce the error in these by increasing the temperature drop associated with the calculations. But at the same time a larger temperature drop means a higher temperature in the lower part of the block. Thus, the thickness of the constantan film is selected such that it has the maximum thickness which maintains the lower thermocouple junction temperature within the range specified for a copper constantan thermocouple. For all experiments in this study, a constantan film thickness of 0.127 mm was used. The very low thermal conductivity of constantan as compared to the copper block also reduces any temperature variations in the copper blocks in the radial direction near the constantan strip. Thus the temperature profiles on both surfaces of the constantan strip are flat even if there are some temperature variations on the heat transfer surface. This allows the integral thermocouple to estimate the average surface temperature rather than the centerline temperature which is measured by the ordinarily used methods. The error analyses for the thermocouple assembly are presented in the Appendix; it suffices to say here that this method of temperature and heat flux measurement is much more accurate than the ordinarily used

method of thermocouples placed in holes drilled in the block. The integral thermocouple calibration and corrections are provided later on in this chapter.

3.2 Heater Block Fabrication

The heater block is made by silver soldering a thin strip of constantan between the upper copper block (containing the heat transfer surface) and the lower copper block (containing the heat source). The two copper pieces are machined separately and then cleaned in an ultrasound cleaner. The ultrasound vibrations cause cavitation on the surface of the blocks and thus clean the surfaces of any grease or other impurities. The cleaned blocks are then arranged as shown in Figure 3.1, i.e., an arrangement of constantan strip; solder flux and silver solder films are placed between the two blocks to enable soldering of the two pieces to the two surfaces of the constantan strip. Care has to be taken to ensure proper orientation of the blocks. The whole arrangement is then placed in an oven and heated up to 750 °C in order to melt the silver solder. The soldered block is then allowed to cool in the oven in presence of an inert gas to prevent oxidation. The soldered block is then cleaned to remove any traces of oxidation and machined again to remove any silver solder which may have overflowed out of the junctions.

The thermocouple wire connections are made by drilling a

hole each in the upper copper block, the lower copper block and the constantan film and attaching the corresponding thermocouple wire by means of small screws. The resulting arrangement shown in Figure 3.1 has three wire connections, the upper copper block, the middle constantan film and the lower copper block. The upper copper block and the constantan strip form the upper thermocouple junction and the lower block forms the lower thermocouple junction with the constantan strip.

3.3 Integral Thermocouple Calibration and Corrections

The temperature readings from the integral thermocouples have to be corrected for the heat flux existing across the silver solder present in the junction. As shown in Figure 3.2 the copper-silver-constantan assembly can be considered equivalent to two thermocouples, constantan-silver and silver-copper, in series. The voltage recorded by the data acquisition system is the sum of the voltages due to the two thermocouples in series as mentioned above.

The exact measurement of temperature requires the individual calibration of both the silver-copper and silver-constantan thermocouples. The calibration was carried out by constructing the two thermocouples mentioned above and calibrating them with reference to a copper-constantan thermocouple. Figure 3.3 shows the calibration curves for the three thermocouples mentioned above. The results presented in

Table 3.1 show the coefficients of the polynomial fit for the individual thermocouples. The thermocouple voltage can be written in terms of these expansion coefficients as :

$$V = a_0 + a_1T + a_2T^2 + \qquad + a_7T^7$$

where :

V = Thermocouple voltage in Volts

T = Temperature in degrees Celsius

The corrected heat flux can then be written as:

$$q'' = k_{ag}\frac{T_1 - T_2}{\Delta x_{ag}} = k_{cn}\frac{T_2 - T_3}{\Delta x_{cn}} = k_{ag}\frac{T_3 - T_4}{\Delta x_{ag}} \qquad (3.1)$$

From the first equality :

$$\frac{k_{ag}}{\Delta x_{ag}}T_1 - \left(\frac{k_{ag}}{\Delta x_{ag}} + \frac{k_{cn}}{\Delta x_{cn}} \right)T_2 + \frac{k_{cn}}{\Delta x_{cn}}T_3 = 0 \qquad (3.2)$$

From the second equality :

$$T_1 - T_2 - T_3 + T_4 = 0 \qquad (3.3)$$

Since the instruments measure the sum of the voltages of the two thermocouples as mentioned earlier, we get :

$$V(T_1) + V(T_2) = V_{lower} \qquad (3.4)$$

$$V(T_3) + V(T_4) = V_{upper} \qquad (3.5)$$

Equations 3.2 through 3.5 give four equations for four

unknowns, knowing the relations between voltage and temperature(which are available from the calibration) we can determine the four unknown temperatures by Gauss-Siedel iterative scheme. This was done by a computer program which was used to determine the unknown temperatures and plot out the heat flux vs. temperature curve.

The temperature on the surface was obtained by extrapolation using the expression :

$$T_{surf} = T_4 - q'' \frac{\Delta x_{cu}}{k_{cu}} \tag{3.6}$$

3.4 Surface Preparation

a) Surface Material: In all, three surface materials were tested. The first was a oxygen free copper surface (the block material). The surface was polished only in one direction using 14-μm-grit emery paper such that it had a definite "Lay" [32]. The second surface was prepared by electroplating the copper surface with nickel. The thickness of the coating being minimal, the temperature drop across it can be neglected and it can be assumed that the surface temperature predicted for the bare copper surface will be accurate enough for analysis. The third surface was similarly prepared by electroplating 24 carat gold over the nickel surface; again the thickness of gold coating was negligible (roughness values for the three surfaces are comparable, indicating similar roughness conditions;

data are provided in the "Results" section).

b) Surface Roughness: For the surface roughness part of the experiments, the surface was polished successively with no. 600 emery paper, no. 2-0 emery paper, 14-μm-grit emery paper and 0.3-μm lapping compound. Each of these roughnesses were studied during the experiments.

3.5 Experimental Set-up

The schematic diagram for the experimental set-up is shown in Figure 3.4. The temperature controller monitors the temperature of a thermocouple attached to the upper part of the block, maintaining it at some preset value by sending a control signal to the phase-angle SCR power supply, which in turn regulates the power to the quartz lamps by varying the phase angle on each AC cycle proportional to the control signal. In the event of an overshoot in the temperature of the block, an alarm disconnects the power to the heaters. The current and the voltage supplied to the lamps are continuously indicated by the panel meters and recorded by the data acquisition system.

3.6 Spray System

An air atomizing nozzle is used to provide a homogeneous droplet spray over the cooling surface (9 mm x 9 mm). A thin annular liquid stream of distilled and

deionized water is injected into the path of an accelerating jet of air. Through surface shear forces the air jet atomizes the water into small droplets, and imparts momentum to them. A water distillation and deionization system supplies the water to a small storage tank from where it is pumped to the nozzle via a magnetic drive pump. A needle valve is used to control the water flow rate and a digital manometer in the line is used to measure the flow rate. The digital manometer measures the pressure drop across an orifice; this pressure drop is calibrated against the flow rate using a graduated cylinder and a stop watch.

The air at atmospheric pressure has a relative humidity (relative humidity = $\frac{p_v}{p_{vs}} \times 100$, where, p_v is the partial pressure of water vapor in the air, and, p_{vs} is the partial pressure of water vapor in saturated air at the same temperature) of 60%; when it is compressed to 70 psi, the partial pressure of water vapor increases due to the increase in pressure, the increase in temperature of compressed air is not sufficient to maintain the same relative humidity and simple calculations show that some water vapor will condense because the relative humidity can only go up to 100%. Thus the supplied compressed air at 70 psi is saturated with water vapor; an expansion valve is used between the air supply and the nozzle inlet to reduce the air pressure entering the nozzle and this serves to control the air flow rate through the nozzle. The reduction in the air pressure first due to the expansion valve and

later the nozzle reduces the relative humidity of the air ejected from the nozzle to about 30% (calculated). Thus, even though the supplied air is totally saturated, the air coming out from the nozzle is relatively dry. An air flow meter between the expansion valve and the nozzle inlet measures the air flow rate and a pressure gauge is used to measure the static pressure of the air entering the nozzle inlet.

3.7 Data Acquisition

A computer aided data acquisition system was used in the experiments. An IBM PC was used to program and control a Fluke 2280 data acquisition system; the system was programmed to record the readings from the integral thermocouples every 10 seconds. The lamp voltage and current, the digital manometer reading and air pressure are monitored continuously by the corresponding instruments and also recorded by the data acquisition system every 2 minutes. It should be noted that the data acquisition system records the integral thermocouple readings in the form of temperature assuming a copper-constantan thermocouple and does not measure the voltage directly. During the final processing of the data, this temperature is converted into the appropriate voltage using the calibration polynomial for the copper-constantan thermocouple; the voltage thus obtained is then used to calculate four temperatures as explained earlier.

3.8 Procedure

Using the air atomizing nozzle spray system, water was sprayed onto the surface at varying air and water flow rates; the nozzle height above the surface was kept fixed at 22 mm for the whole set of experiments. The block was gradually heated to higher temperatures by increasing the set-point temperature of the controller, the surface temperature was thus increased till dryout for most cases. During this process the data aquisition system records the output from the two thermocouples formed by the constantan film and the upper and lower part of the copper block. This output is then corrected for the silver solder present in the junction as explained earlier. The corrected temperature of the lower and the upper thermocouple junction is then used to obtain the heat flux and the average surface temperature by extrapolation. Thus, a plot for the heat flux vs. the surface temperature can be obtained for various spray conditions.

For each surface material and surface roughness, experiments were performed for different spray configurations obtained by :

a) Varying the water flow rate

b) Varying the air flow rate

In all, three different water flow rates and three air flow rates were used in all possible combinations for each set of experiments. The following chapter presents the results obtained from the experiments.

Chapter 4

Results

4.1 Effect of Water Flow Rate

Figure 4.1 shows the effect of varying the water flow rate at a constant air flow rate of 0.16 l/sec for a copper surface polished with 14-μm emery paper. It can be seen that increasing the water flow increases the heat flux at any given temperature. This is probably due to the increased convection heat transfer arising from increased droplet density. It was seen that there occurred a saturation of heat flux, (i.e., there was no increase in heat transport for further temperature rise of the surface) in the case of water flow rate of 1.0 l/hr. This was due to the fact that for this flow rate the spray density is higher in the center as compared to the outer part of the spray cone; therefore, the outer parts of the surface receive relatively less water. Due to this, the surface starts drying out at the edges first and this causes the local temperature at the outer parts to shoot up while the heat flux remains almost the same; since the thermocouples measure the average temperature, an increase in temperature at near constant heat flux is observed. It is also seen that as the water flow rate increases the slope of curve reduces; this indicates that at higher flow rates the increased convection causes a decrease in phase change by

depressing nucleation. Figures 4.2 and 4.3 show the effect of water flow rate at 0.25 l/sec and 0.32 l/sec of air, respectively; the trends observed are similar to those explained earlier.

4.2 Effect of Air Flow Rate

Figure 4.4 shows the effect of varying the air flow rate at a water flow rate of 1.0 l/hr on the heat flux for a copper surface polished with 14-μm emery paper. The heat flux at any temperature increases with increasing air flow rate; this is due to two reasons: 1) a higher air flow rate increases the momentum of the droplets and, thereby causes an increase in convection resulting from the droplets impacting the thin liquid film 2) a higher air flow rate causes the liquid film to thin out due to the stagnation air flow field and thus reduces the thermal resistance due to conduction imposed by the liquid film 3) a higher flow rate of air decreases the partial vapor pressure near the free surface of the liquid film and thereby enhances evaporation by reducing the saturation temperature. Figure 4.5 shows similar trends for a water flow rate of 2.0 l/hr.

An important point to note in all these results is that even at surface temperature below 100°C there is some phase change contribution to the heat flux. Referring to Fig. 4.4 again, at an air flow rate of 0.32 l/sec, the heat flux at 80°C is 115 W/cm^2, even if we assume that the heat transfer efficiency is 100% the sensible heating is:

$$q'' = C_p \cdot (T_{surf} - T_{water}) \cdot \dot{m}_{water}$$

$$= 4175.0 \times (80-24) \times 1.0/3600$$

$$= 65 \text{ W}$$

Since this heat is removed from a 9.0×9.0 mm square, we have the maximum possible sensible heat removal = 80 W/cm^2. Therefore, there is definitely some evaporation much before 100°C; hence, the hypothesis that phase change contribution is significant at negative superheats is confirmed. This phase change takes place from the free surface of the liquid film due to the intense convection caused by the impinging droplets.

As seen from Figures 4.4 and 4.5 this evaporation becomes more significant as the air flow rate is increased. This is because an increase in air flow rate causes an increase in all of the effects mentioned earlier.

Comparing the effect of air flow rate and the water flow rate it can be seen that the water flow rate does not have as much effect on the heat flux as the air flow rate for the temperature range, 100 °C to 160 °C. In fact, in this temperature range the water flow rate has hardly any effect; this is because an increase in water flow rate causes an increase in the liquid film thickness which will, in effect, reduce the evaporation from the free surface of the film, but at the same time the increase in water flow rate will result in an increase in heat removed by sensible heating of the liquid. These effects seem to cancel each other out with the result that very little change in heat

flux is observed with an increase in water flow rate.

4.3 Effect of Coolant Temperature

Effect of coolant temperature at a flow rate of 1.0 l/hr on a copper surface polished with 14-μm emery paper is shown in Figure 4.6. As seen, the heat flux for the higher temperature coolant is lower at first; this is because in the initial stages the heat transfer is mainly sensible heating of the coolant and this will be lower for the coolant at higher temperature. At around 100°C the slope of the curve for the hotter coolant increases as compared to the room temperature coolant. This is because the hotter coolant requires lower superheat for nucleation and hence more nucleation takes place as compared to the coolant at room temperature. As the temperature of the surface increases, the higher temperature coolant spray case reaches CHF earlier than the cooler fluid spray. The critical heat flux is lower as it lacks the sensible heating part (which makes up about 10-15% of the total heat flux) of the heat transfer process as compared to the cooler fluid spray.

Figures 4.7 and 4.8 show the effect of increased coolant temperature for a flow rate of 2.0 l/hr and 4.0 l/hr, respectively. The trends are similar to those for the 1.0 l/hr case. The effect is more pronounced for 4.0 l/hr case. As shown in Fig. 4.8 the curve for coolant at room temperature shows a very gradual change in slope indicating little nucleation, but as the temperature of the fluid is

increased, a much more pronounced increase in slope is observed near 100°C indicating a greater effect of nucleation on the heat transfer. For temperatures below 100°C the slope of the curve for higher temperature coolant is slightly higher than that for lower temperature coolant. This is because of the increased evaporation due to higher temperature of the coolant. At higher temperatures too, this increased evaporation is expected to be one of the factors for increased heat transfer.

4.4 Contact Angle Measurements

As mentioned earlier three different surface materials were used for studies concerning the effects of wettability on spray cooling. It is well known that gold has a very high contact angle (all contact angles are with reference to water) as compared to copper and nickel. Nickel in fact has almost the same contact angle as copper [17]. Contact angle measurements were done using a contact angle viewer which provides a magnification of 40X. To measure the contact angles of the surfaces used in the experiments, a thin strip of copper (about 3 inches long) was coated with nickel for one-third of its length, the next one-third was left bare and the last section was coated with gold. The process used for the coatings was exactly the same as that used in the experiments. The surface was then cleaned with methanol and a drop of water was put on each of the three sections. The instrument was then used to view a magnified profile of the

drop and measure the static contact angle by aligning a protractor tangential to the drop at the liquid/solid interface. Thus all the three surfaces were given identical treatment and hence the relative values of the contact angles are a true representation of the actual differences in the contact angles. The results of the contact angle measurements are presented in Figure 4.9; four sets of measurements are presented here. It can be seen that gold has a much higher contact angle as compared to copper and nickel. Although these measurements represent the contact angles at room temperature, the relative magnitudes of the contact angles are not expected to be different at higher temperatures [17]. This is due to the fact that the surface material properties do not change much over the temperature range studied (60 °C - 220 °C), and therefore the change in contact angle with temperature is mainly due to the change in liquid properties. It should be noted that dynamic contact angle is usually much higher than the static contact angle and hence these measurements are not really representative of the actual situation. However, for the purpose of this study it is sufficient to note the relative magnitudes of the contact angles.

Table 4.1 provides the roughness values R_q, R_p of the copper, nickel and gold surfaces prepared with 14-μm emery paper. It is noted that the values of the surface roughnesses are comparable. Here, R_q is the geometric average roughness defined as the root-mean-square of the

roughness heights about a mean line and R_p is the maximum height of the profile above the mean line within the assessment length.

4.5 Contact Angle Effects

Figure 4.10 shows the effect of the contact angle on heat transfer characteristics for a water flow rate of 4.0 l/hr and an air flow rate of 0.16 l/sec. As can be seen there is a definite increase in slope for gold at around 100°C as compared to copper and thereafter the gold surface gives a higher heat flux until at around dryout where all the curves begin to merge. The nickel surface curve lies between gold and copper as would be expected. This leads us to believe that the higher contact angle of gold causes the water to nucleate earlier than ror copper or nickel surface. The critical heat flux is at a lower temperature for gold; this is because a higher contact angle will cause more nucleation thereby causing the formation of the vapor blanket earlier.

Figure 4.11 shows the effect of the surface material at a flow rate of 1.0 l/hr of water, respectively, and at an air flow rate of 0.16 l/sec. A 14-μm emery paper was used for polishing. Again the trends are as mentioned for the case of Figure 4.10. It is observed that at the lower water flow rate the effect was less pronounced than for the higher water flow rate. Three mechanisms come into play in such a comparison:

1) The higher contact angle provides a better possibility for nucleation and hence, enhanced heat removal.

2) The higher contact angle provides a more stable and surface adhering bubble. Hence, the nucleating bubbles are not swept away instantly by the faster flow, but are able to reach some optimum size before ejection. Hence, providing a higher contribution to phase change heat transfer.

3) Due to the subcooling the onset of nucleation is delayed at higher flow rates (100 ^{0}C for 1 l/hr and 110 ^{0}C for 2 l/hr).

Increasing the air flow rate tends to thin out the film and increases the convection thus nucleation is reduced at higher air flow rates. Figure 4.12 shows the effect of increased air flow rate on surface material effect. As can be seen all the three curves are pushed very close together though the gold surface still shows a little higher heat fluxes between 100°C and the CHF region. The critical heat flux is almost the same for all the materials (some scatter appears because of the instabilities in this region).

4.6 Surface Roughness Measurements

As mentioned earlier, four different surface roughnesses were studied. These were the #400-emery-paper polish, #600-emery-paper polish, 14-μm grit emery-paper polish and the 0.3-μm grit polish on a copper surface. The surface profiles for these surfaces were measured (the

surface profiles for the gold and nickel surfaces were also measured) using a diamond tip profilometer; the profiles for the last two surfaces are shown in Figures 4.13 and 4.14.

4.7 Surface Roughness Effects

Experiments were performed on copper surface with the four different surface roughnesses mentioned above. All the results presented up to now referred to surfaces polished with 14-μm-grit emery-paper. The smoothest surface tested was a bare copper surface polished with 0.3-μm-grit polish. As shown in Figure 4.15, something startling happens at around 80 °C for this surface; the heat flux shoots up at near constant temperature and later increase in temperature shows an increase in heat flux (the surface temperature was not increased till dryout for the fear of oxidizing this highly polished surface). As can be seen, the increase is almost 40-50% in heat flux at any temperature above 80°C. This can be explained with the help of Figure 4.16; as seen from the figure, the mean film thickness is directly related to the roughness of the surface, the smoother a surface the lower the film thickness. The steep increase in heat flux is because a very smooth surface provides a liquid film thin enough to evaporate, by enhanced conduction through the liquid film, from the free surface. The low temperature at which this phenomenon takes place is due to the decrease in partial vapor pressure at the free surface caused by the air flow field. This secondary flow of air causes the liquid to

evaporate at a temperature much lower than its saturation temperature at atmospheric pressure. Initially the liquid film can be imagined to be as shown in Figure 4.16; the liquid on the surface of the film evaporates by heat transferred through the film by enhanced conduction. As the liquid evaporates the film thickness will be expected to decrease because lesser liquid stays on the surface. This decrease in liquid film thickness will further augment the heat transfer because of the increasing temperature gradient in the liquid film. This whole process gives rise to the near vertical slope of the heat flux vs. temperature curve.

Figure 4.17 shows a similar effect at a different water flow rate. This phenomenon of a steep rise in heat flux without a substantial change in surface temperature provides the following advantages:

a) a very efficient removal of heat at a very low surface temperature.
b) the heat dissipation can increase by a large amount without altering the surface temperature significantly. This can be of great advantage in applications where varying heat fluxes have to be dissipated, but the temperature has to be maintained constant.

The effect of surface roughness for rougher surfaces (i.e., rougher than the 14-μm-grit polished surface) was also studied and the results are presented in Figure 4.18. It is seen that the effect of roughness is hardly noticeable

for these levels of roughness. A rougher surface has a higher surface area in contact with the liquid and hence for the same heat transfer coefficient will show a higher heat flux per unit projected area. However the liquid film thickness also increases with roughness and this will cause a decrease in heat transfer coefficient at the heater surface. Thus it appears that the effect of increased surface area and the effect of increased average liquid film thickness for a rougher surface cancel each other out. Thus it was seen that the heat transfer dependence on surface roughness is not very strong if the surface is rougher than a 0.3-μm-grit polished surface.

Chapter 5
Conclusions

Based on the experimental results it can be safely concluded that nucleation plays an important role in spray cooling heat transfer. Nonsmooth surfaces having a high contact angle were shown to enhance spray cooling heat transfer by promoting nucleation on the surface. The exact contribution of nucleation to spray cooling though remains uncertain because of the other phase change phenomena involved in the spray cooling process.

It was also shown that evaporation from the free surface of the liquid film is a contributing factor even at low surface temperatures. This evaporation is the result of the combination of three factors:

a) a thin liquid film, which reduces the thermal resistance between the hot surface and the free liquid surface.

b) the intense mixing in the liquid film due to the impacting of high velocity liquid droplets from the spray.

c) the reduction in partial vapor pressure at the free surface due to the stagnation air flow field which results in a decrease in saturation temperature.

The direct evaporation from the free surface of the liquid film leads to extremely efficient heat transfer if

the liquid film is very thin, as in the case of a mirror smooth surface. In such a case heat flux increases extremely fast at near constant temperature. This mode of spray cooling can be very useful in applications where varying amount of heat has to be removed in a very narrow temperature range.

For any particular surface configuration, it was shown that an increase in liquid flow rate (with other conditions remaining the same) causes an increase in heat flux due to the increase in convection caused by increase in droplet density and size. An increase in air flow rate causes the thinning of the liquid film which results in increased evaporation from the free liquid surface thereby resulting in an increase in the heat flux. It was also seen that, comparatively, the air flow rate has more effect on the heat flux than the water flow rate.

The effect of liquid temperature was also examined and it was found that a hotter liquid shows a steeper rise in heat flux with temperature. This is because of the increased phase change made possible by the elevated temperature.

In conclusion it can be said that this study has increased our knowledge of the underlying phenomena in spray cooling. More work needs to be done to fully understand and model the process. Further work in this area should be concentrated on determining the effect of spray parameters like droplet size, distribution and velocity, on the spray

cooling heat transfer. Also the liquid film thickness has to be determined in order to evaluate the relative importance of nucleation and direct evaporation.

References

1 Choi, K.J. and Yao, S.C., "Mechanism of Film Boiling Heat Transfer of Normally Impacting Spray," **Int. J. Heat Mass Transfer**, vol. 30, No. 2, pp. 311-318, 1987.

2 Goldstein, M.E., Yang, Wen-Jei and Clark, J.A., "Momentum and Heat Transfer in Laminar Flow of Gas With Liquid-droplet Suspension Over a Circular Cylinder," **J. Heat Transfer**, pp. 185-194, 1967.

3 Pais, M.R., Tilton, D., Chow, L.C. and Mahefkey, E.T., "High Heat Flux Low Superheat Evaporative Spray Cooling," **AIAA-89-0241**, AIAA 27th Aerospace Sciences Meeting, Reno, Nevada, 1989.

4 Pais, M.R., Chow, L.C., and Mahefkey, E.T., "Surface Roughness and Its Effects on the Heat Transfer Mechanism in Spray Cooling," **ASME WAM**, San Fransisco CA, HTD-Vol. 119, 1989.

5 Cole, R., "Boiling Nucleation," **Advances in Heat Transfer**, Vol. 10, p. 85, 1974.

6 Berenson, P.J., "Experiments on Pool Boiling Heat Transfer," **Int. J. Heat Mass Transfer**, Vol. 5, pp. 985-999, 1962.

7 Kurihara, H.M. and Myers, J.E., "The Effects of Superheat and Surface Roughness on Boiling Coefficients,". **AIChE J.**, Vol. 6, No. 1, pp. 83-91, 1960.

8 Webb, R.L., "The Evolution of Enhanced Surface Geometries for Nucleate Boiling," **Heat Transfer**, Vol. 2, No. 3-4, 1981.

9 Bonacina, C., Del Guidice, S., Comini, G., "Dropwise Evaporation," **Journal of Heat Transfer**, Vol. 101, pp. 441-446, 1979.

10 Toda, S., "A Study of Mist Cooling," **Heat Transfer-Japanese Research**, Vol. 1(3), pp. 39-50, 1972.

11 Eastman, G.Y., Ernst, D.M., "High Power Density Evaporative Cooling," Final Report, Air Force Weapons Lab., Kirtland AFB NM, 1982.

12 Tilton, D.E., "Spray Cooling," Ph.D. Dissertation, Univ. of Kentucky, 1989.

13 Collier, J.G., "Convective Boiling & Condensation," McGraw-Hill publications, 1972.

14 Jussin, E., **Stopping Time: The photographs of Harold Edgerton**, Harry N. Abrams Inc., New York, 1988.

15 Defay, R., Progogine, I., Bellemans, A., and Everett, D.H., "Surface Tension and Adsorption," John Wiley & Sons, New York, 1966.

16 Bankoff, S.G., "Entrapment of Gas in the Spreading of a Liquid Over a Rough Surface," **AIChE J.**, pp. 24-26, 1958.

17 Griffith, P., and Wallis, J.D., "The Role of Surface Conditions in Nucleate Boiling," **Chem. Engrg Progr Symp Ser**, Vol. 56, No. 30, pp. 49-63, 1960.

18 Pais, M.R. and Singh, S.N., "A Fourier Analysis Approach for Surface Definition and the Effect of Roughness on the Local Convective Heat-transfer Coefficient as Related to Ice Accretion," AIAA 26th Aerospace Sciences Meeting, Reno NV, **AIAA-88-0117**, 1988.

19 Dhir, V.K., and Tung, V.X., "A Thermal Model for Fully Developed Nucleate Boiling of Saturated Liquids," ASME Winter Annual Meeting, Chicago, Illinois, 1988.

20 Mesler, R., "A Mechanism Supported by Extensive Experimental Evidence to Explain High Heat Fluxes Observed During Nucleate Boiling," **AIChE J.**, Vol. 22, No. 2, pp. 246-252, 1976.

21 Hospeti, N.B., and Mesler, R.B., "Vaporization at the Base of Bubbles of Different Shape During Nucleate Boiling of Water," **AIChE J.**, Vol. 15, pp. 214-219, 1969.

22 Berenson, P.J., "Transition Boiling Heat Transfer from a Horizontal Surface," MIT Heat Transfer Lab., **Tech. Rep # 17**, 1960.

23 Cooper, M.G., and Merry, J.M.D., "A General Expression for the Rate of Evaporation of a Layer of Liquid on a Solid Body," **Int. J. Heat Mass Transfer**, Vol. 16, pp. 1811-1815, 1973.

24 Yu, C.L., and Mesler, R.B., "A Study of Nucleate Boiling Near the Peak Heat Flux Through Measurement of the Transient Temperature," **Int. J. Heat Mass Transfer**, Vol. 20, pp. 827-840, 1977.

25 Faneuff, C.E., McLean, E.A., and Scherrer, V.E., "Some Aspects of Surface Boiling," **J. Appl. Phys.**, Vol. 29, No. 1, pp. 80-84, 1958.

26 Hsu, Y.Y., "On the Size Range of Active Nucleation Cavities on a Heating Surface," **J. Heat Transfer**, pp. 207-216, 1962.

27 Mesler, R., Mailen, G., "Nucleate Boiling in a Thin Liquid Film," **AIChE Journal**, Vol. 23, pp. 954-957, 1977.

Appendix

Error Analysis

The integral thermocouple assembly provides a measurement of the temperature at the first point of contact between the copper block and constantan strip on the side the lead is taken from the constantan strip. Thus it is essential that temperature be uniform all over the cross section at the planes of the copper-constantan junctions. To check this a finite element analysis was performed on the block subject to a constant heat flux and a nonuniform surface temperature. The surface temperature at the outer edges was assumed higher because of the lower spray density, a parabolic temperature profile was assumed. It was seen that for a temperature variation of up to 25°C, the temperature profile becomes uniform near the copper-constantan junction due to the very low conductivity of constantan. Since the spray density variations are not very large a temperature variation of even 20 °C cannot be expected unless dryout occurs at the outer edges in which case the temperature difference could be appreciably larger. Thus the integral thermocouple set-up is suitable for measurements at least up to the point where the outer parts of the surface begins to dry out.

The uncertainty in the heat flux and temperature prediction is calculated based on the following formula for

28 Corty, C. and Foust, A.S., "Surface Variables in Nucleate Boiling," **AIChE, Chem. Engrg. Prog. Series**, Vol. 51, No. 17, pp.1-12, 1955.

29 Liaw, S.P. and Dhir, V.K., "Effect of Surface Wettability on Transition Boiling Heat Transfer from a Vertical Surface," 8th Int. Heat Transfer Conference, San Fransisco CA, Vol. 4, pp. 2031-2036. Hemisphere, Washington D.C., 1986.

30 Tong, W., Bar-Cohen, A., Simon, T.W. and You, S.M., "Contact Angle Effects on Boiling Incipience of Highly Wetting Liquids," **Int. J. Heat Mass Transfer**, Vol 33, No. 1, pp. 91-103, 1990.

31 Maracy, M. and Winterton R.H.S., "Hysteresis and Contact Angle Effects in Transition Pool Boiling of Water," **Int. J. Heat Mass Transfer**, Vol. 31, No. 7, pp. 1443-1449, 1988.

32 Marks' Standard Handbook for Mechanical Engineers, Chapters 4 and 13, 8th ed., McGraw Hill, New York, 1978.

uncertainty in measurement of a function f(x,y,z):

$$\Delta f(x,y,z) = \left\{\left(\frac{\partial f}{\partial x}\cdot\delta x\right)^2 + \left(\frac{\partial f}{\partial y}\cdot\delta y\right)^2 + \left(\frac{\partial f}{\partial z}\cdot\delta z\right)^2\right\}^{1/2}$$

Heat flux calculations have to be done taking into consideration the silver solder present in the copper constantan junctions; the details of this calculation are given in Chapter 3, for the purpose of uncertainty analysis a simpler model is considered. The silver solder correction is ignored to get an approximate bound on the uncertainty. The analysis is done using the data given below:

Conductivity of copper	390 W/m K,	± 1.0 W/m K
Conductivity of constantan	21.12 W/m K	± 0.5 W/m K
Temp diff between thermocouples	50.0 °C,	± 2.8 °C
Distance between thermocouples	0.0127 cm	± 0.0005 cm
Distance between upper thermocouple junction and the upper surface	0.4762 cm	± 0.0005 cm

Using the given uncertainty analysis formula and the above data the uncertainty in heat flux is found to be 8.3% at a heat flux of 850 W/cm². The resulting uncertainty in surface temperature is 8.4% .

The uncertainty in air pressure is 2 psi and that in air flow rate is about 5%. The uncertainty in the flow rate of water is obtained from the method used for calibration; the flow rate is calibrated using a 100-cc-graduated

cylinder and a stop watch. The uncertainty in measured volume was ± 2 cc, the uncertainty in time was ± 0.2 s. This results in a water flow rate uncertainty of about ± 20 cc/hr.

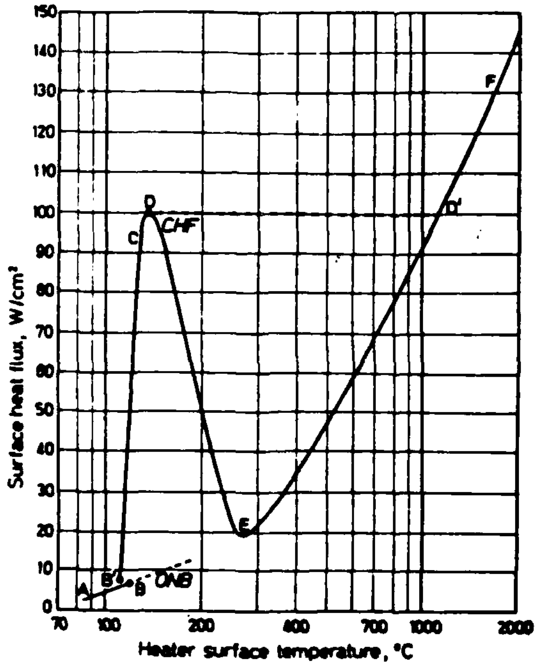

D Critical Heat Flux Point
E Leidenfrost Point
B'Onset of Nucleate Boiling

Figure 2.1 Pool Boiling Curve for Water

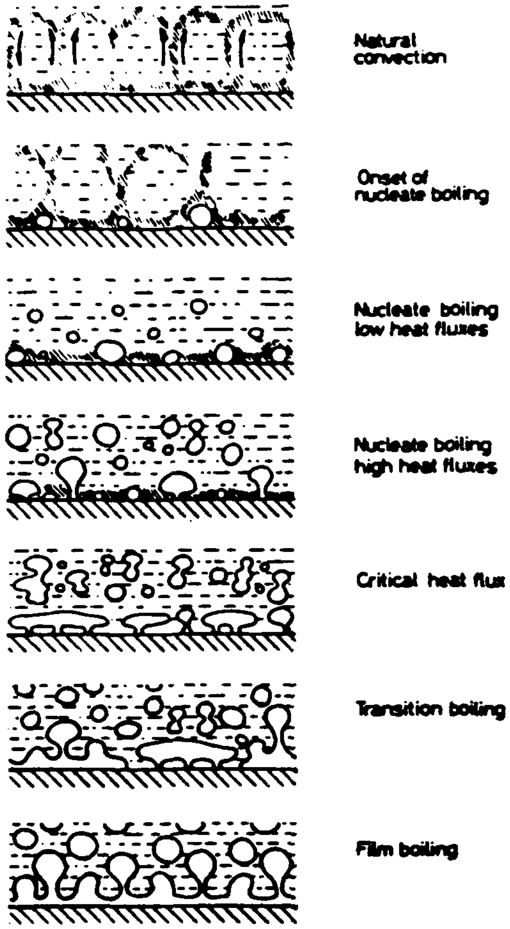

Figure 2.2 Stages of Pool Boiling

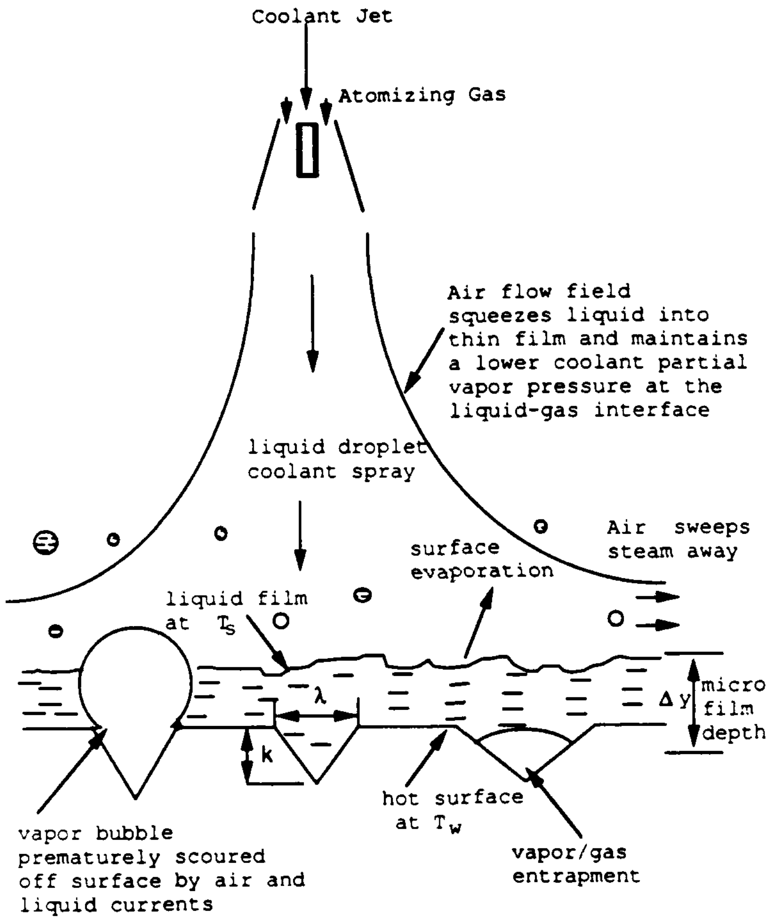

Figure 2.3 Physics of Spray Cooling

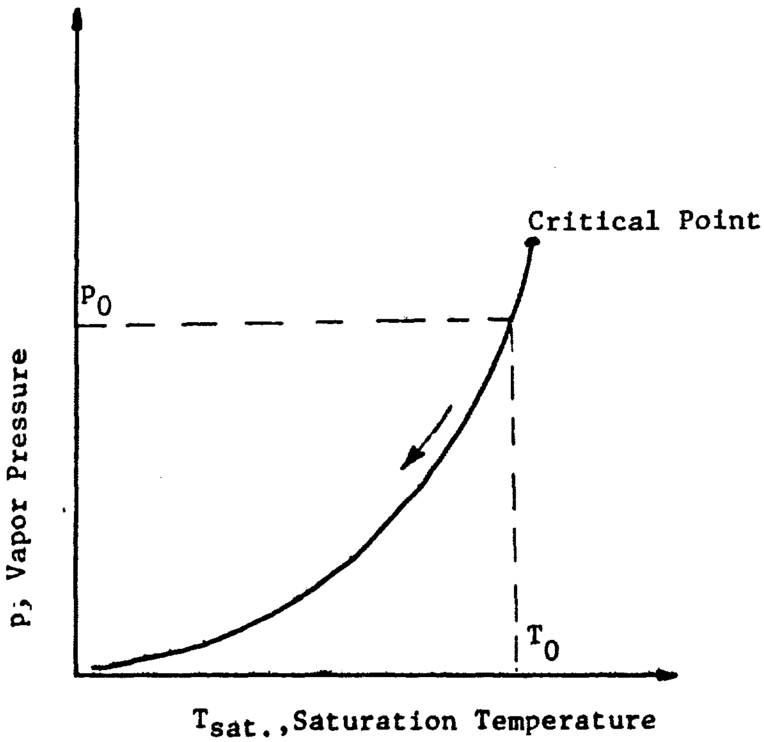

Figure 2.4 Partial Vapor Pressure vs. Saturation Temperature Curve

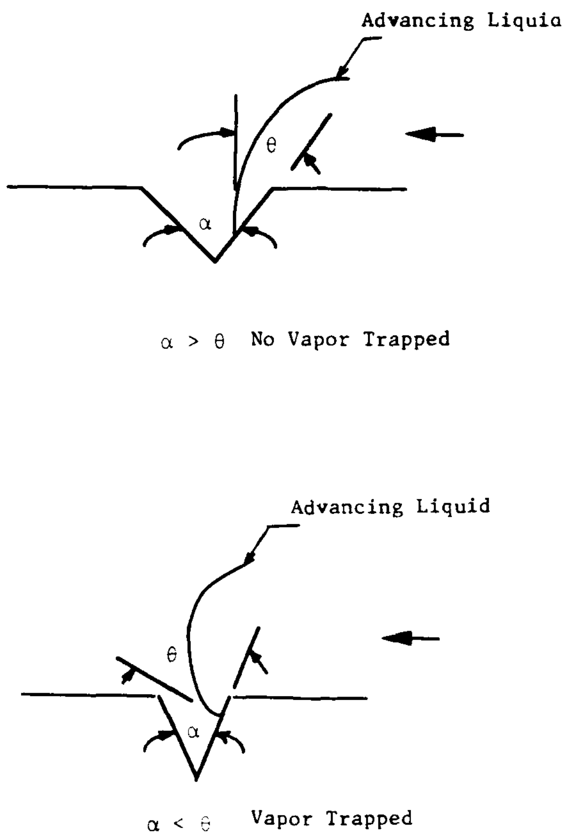

Figure 2.5 Vapor Entrapment in Cavities

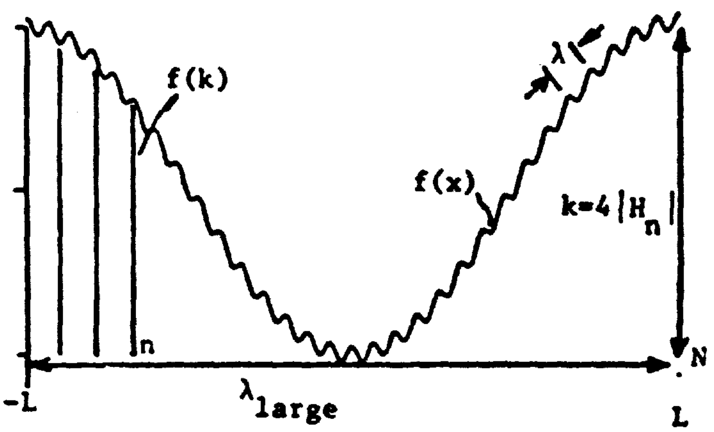

Figure 2.6 Surface Line Profile

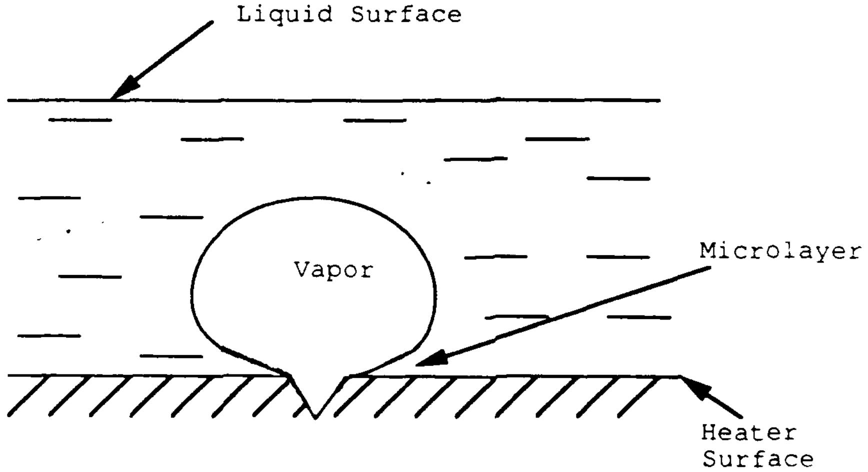

Figure 2.7 Microlayer in Bubble Growth

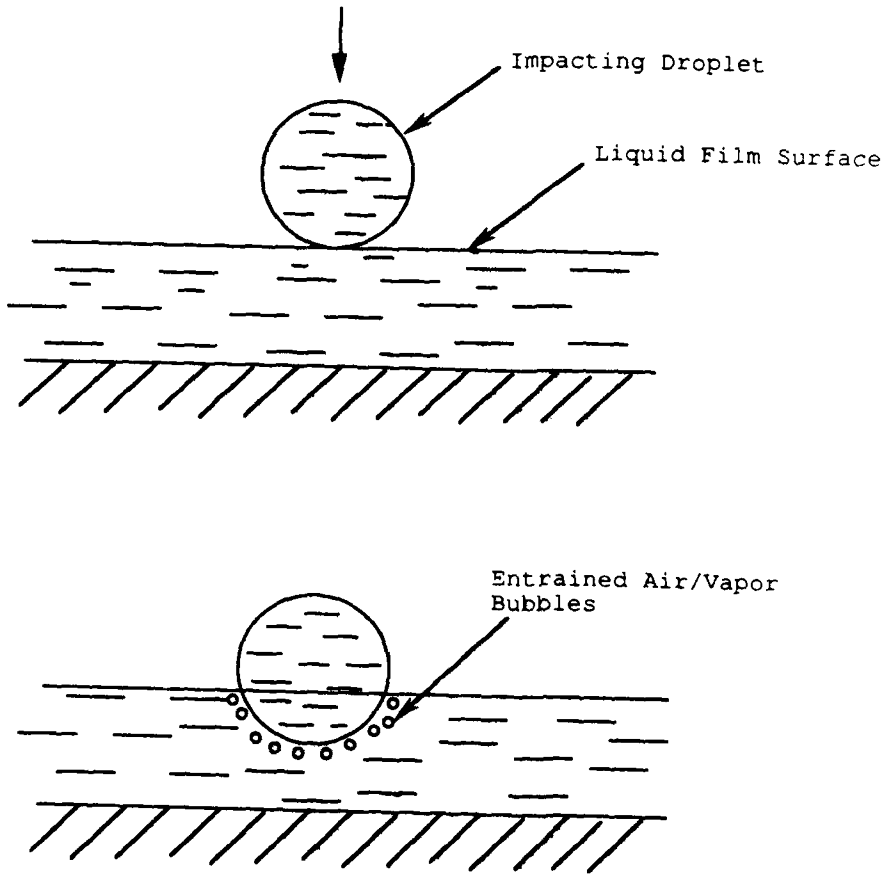

Figure 2.8 Secondary Nucleation

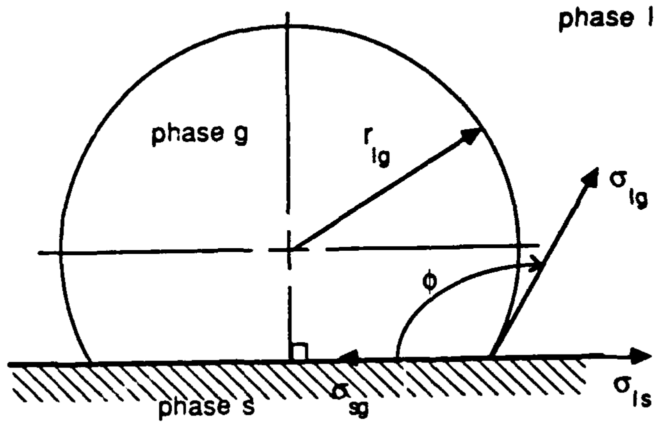

Figure 2.9 Critical Nucleus at Liquid-Solid Interface

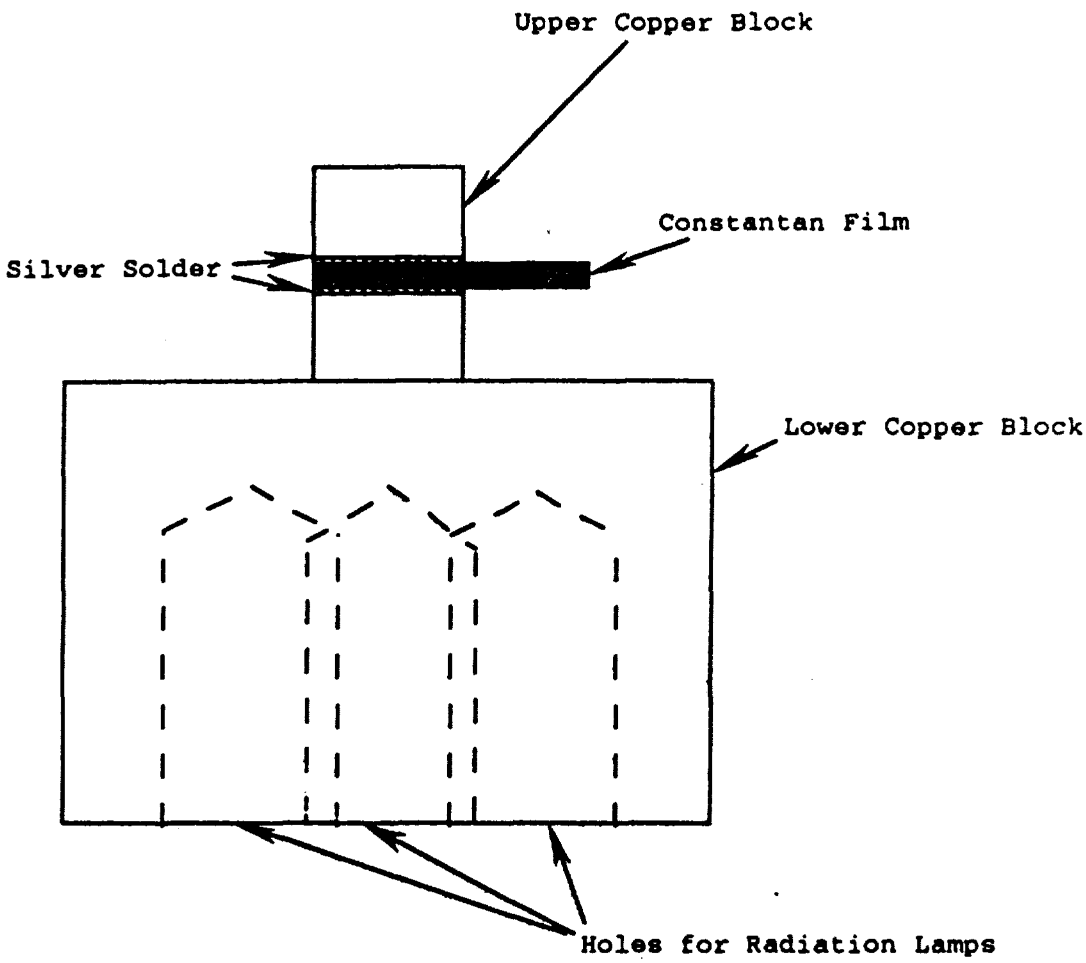

Figure 3.1 Heater Block

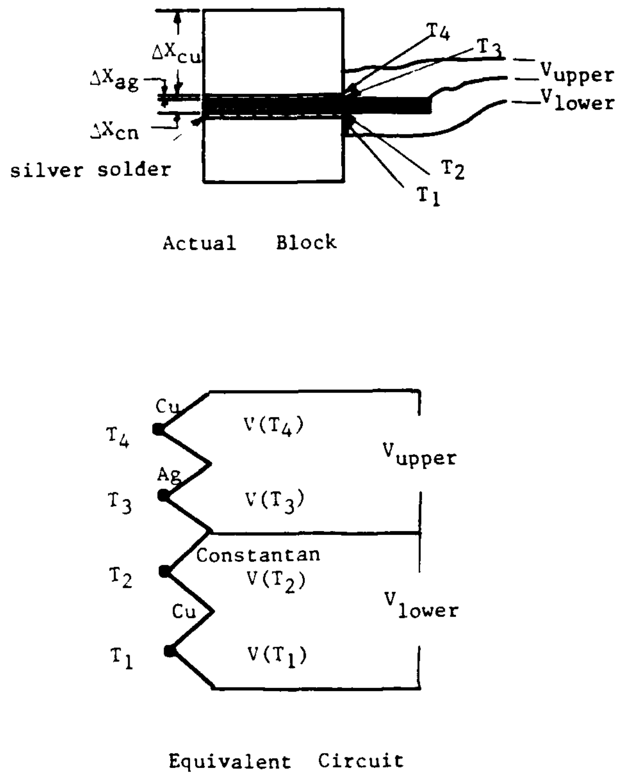

Figure 3.2 Integral Thermocouple Equivalent Circuit

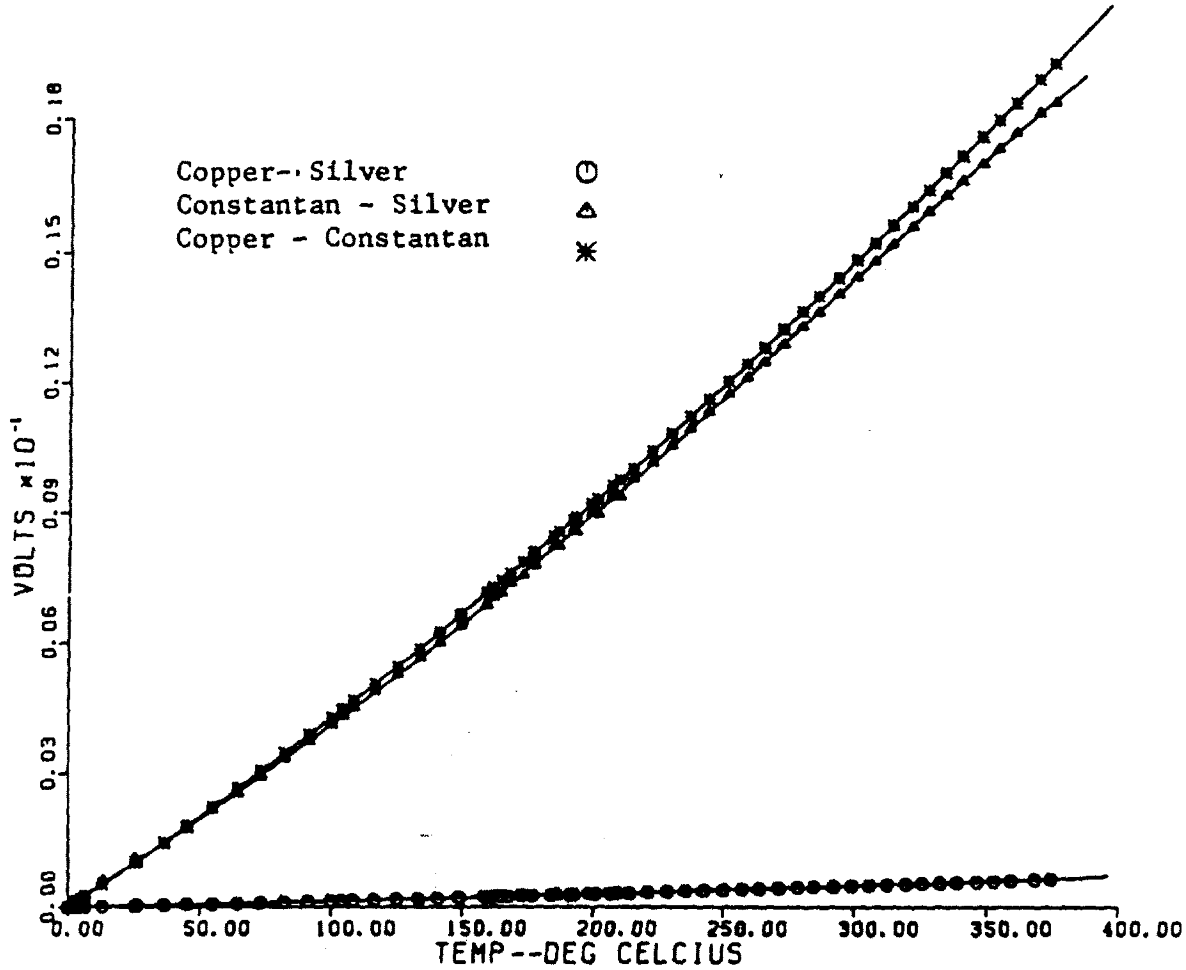

Figure 3.3 Thermocouple Calibration Curves

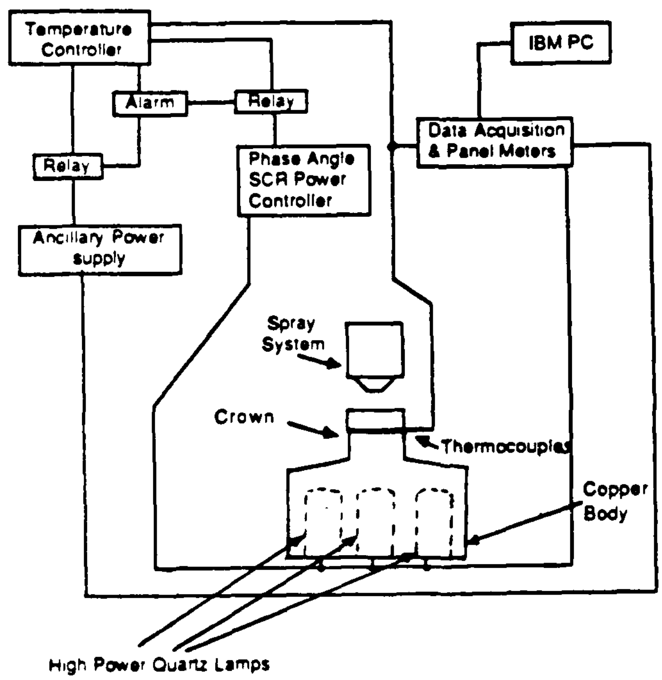

Figure 3.4 Experimental Set-up Schematic

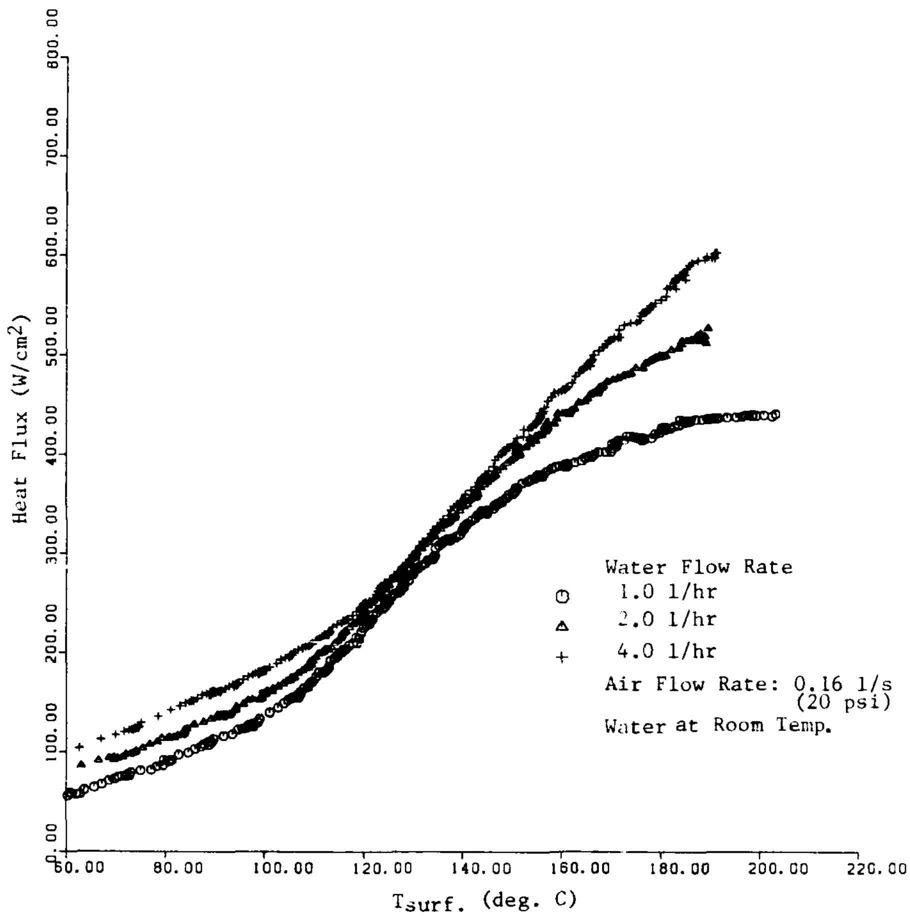

Figure 4.1 Effect of Water Flow Rate - 1

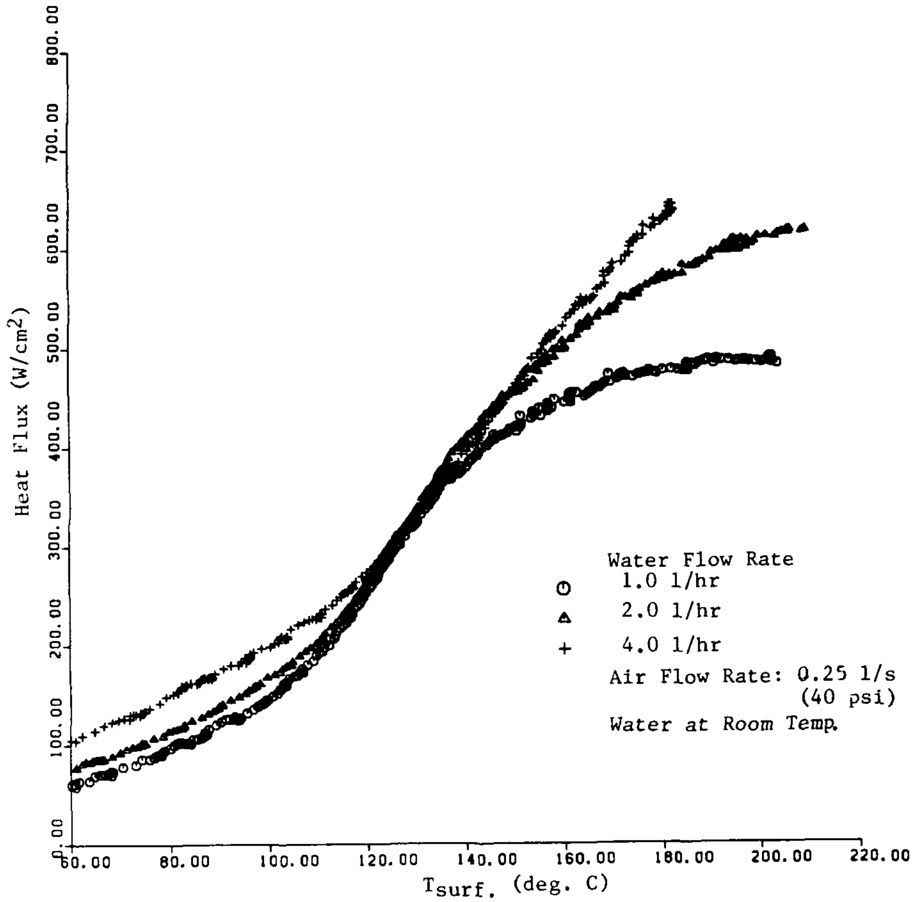

Figure 4.2 Effect of Water Flow Rate - 2

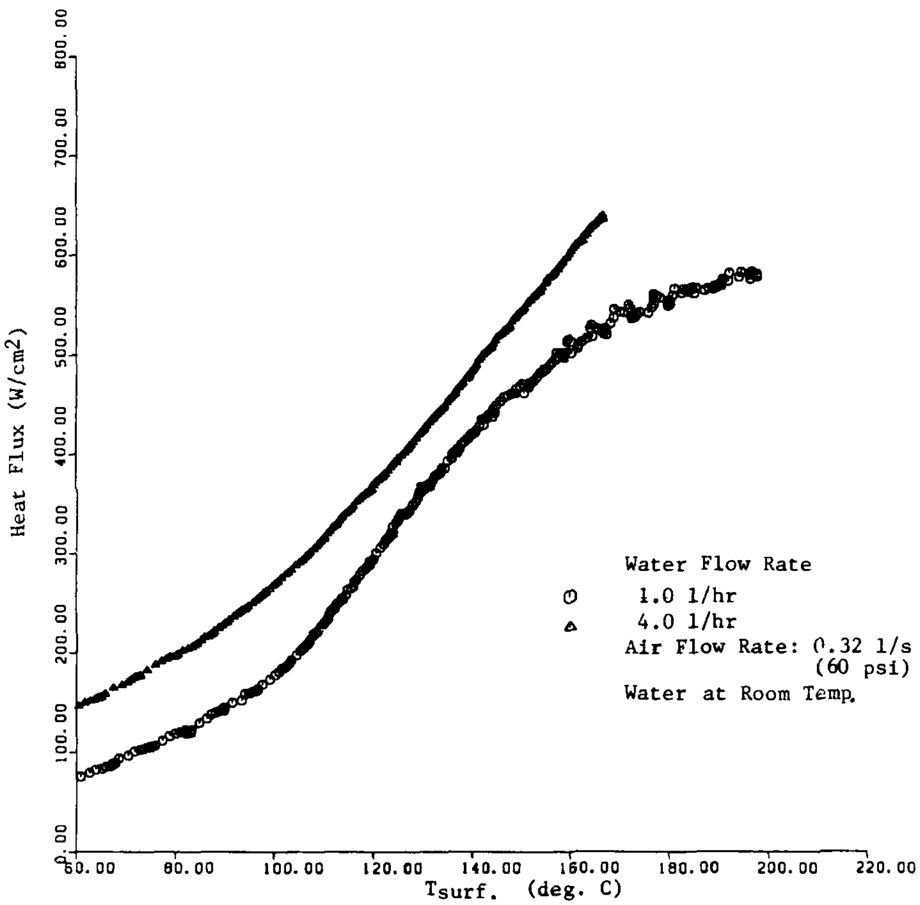

Figure 4.3 Effect of Water Flow Rate - 3

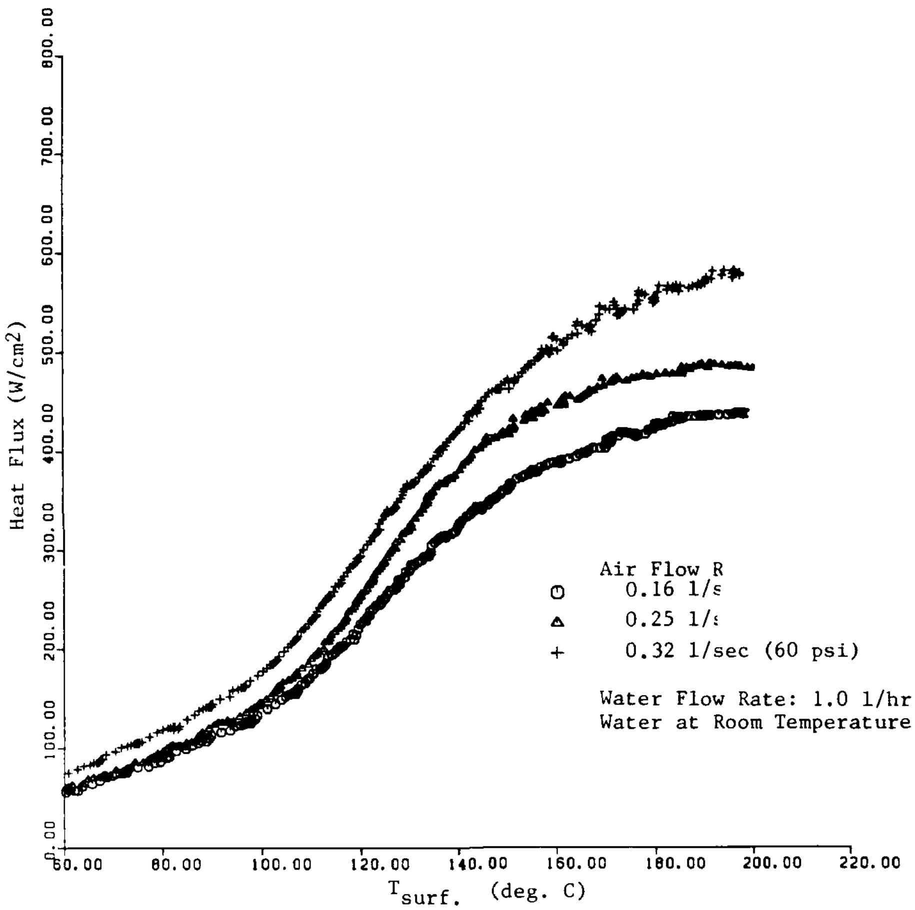

Figure 4.4 Effect of Air Flow Rate - 1

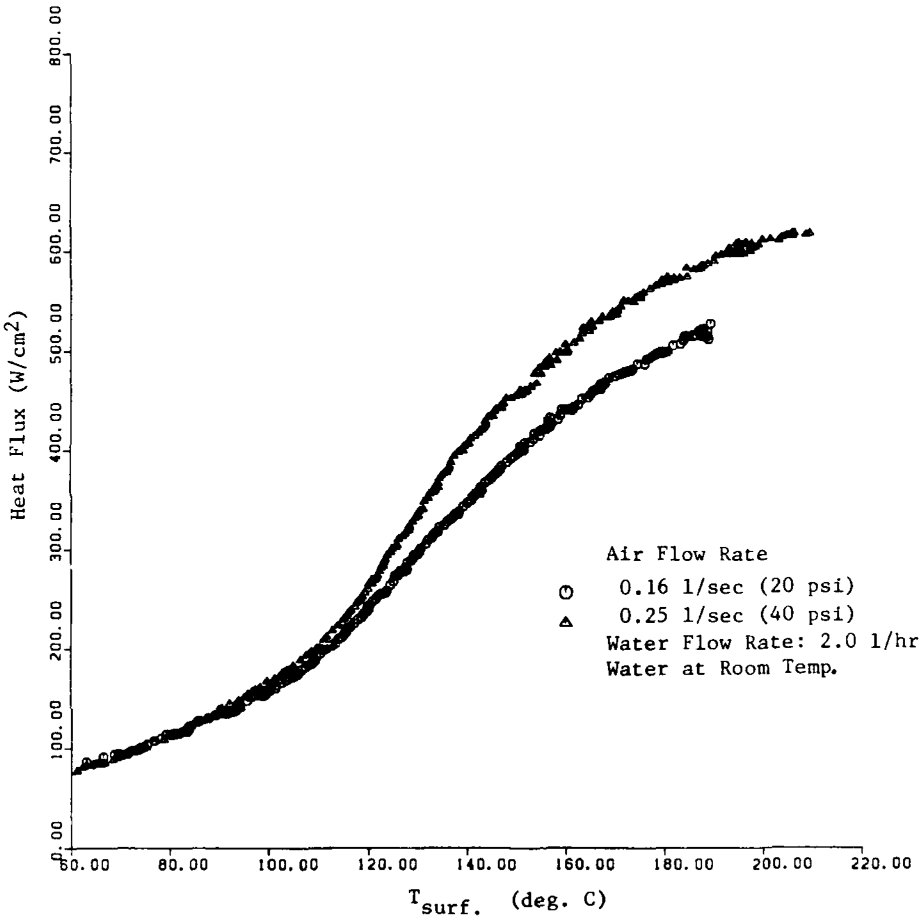

Figure 4.5 Effect of Air Flow Rate - 2

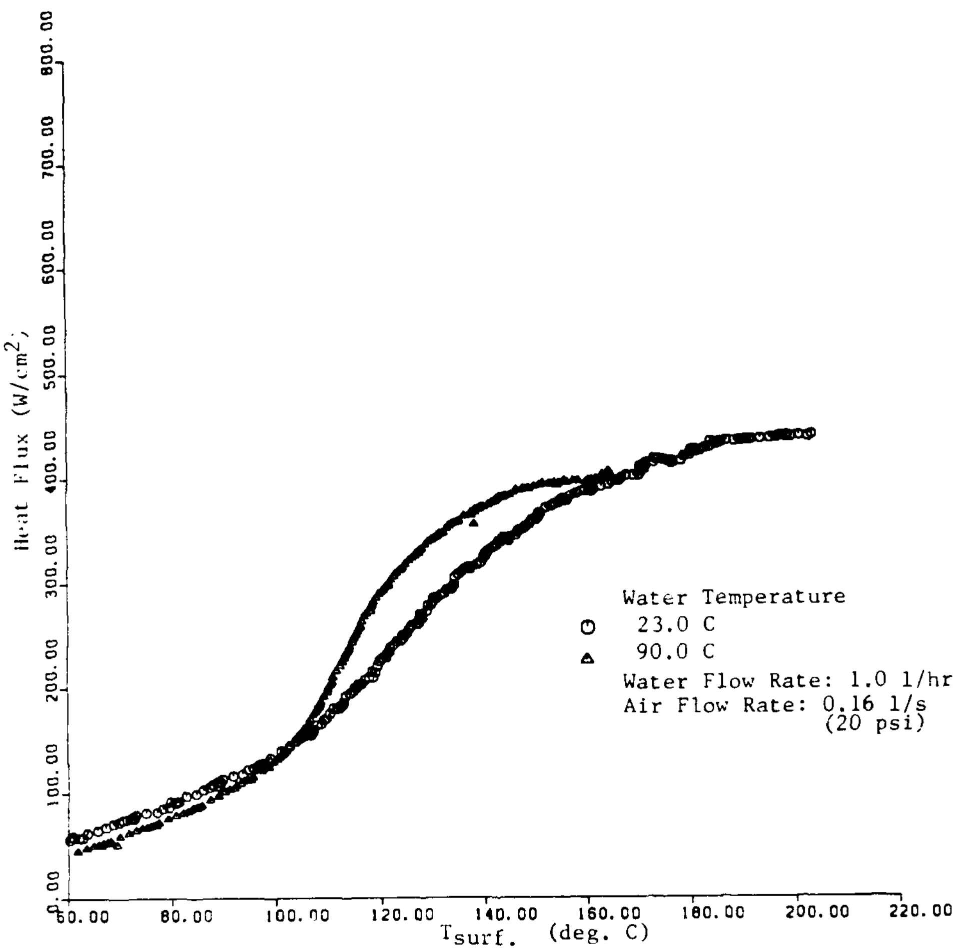

Figure 4.6 Effect of Coolant Temperature - 1

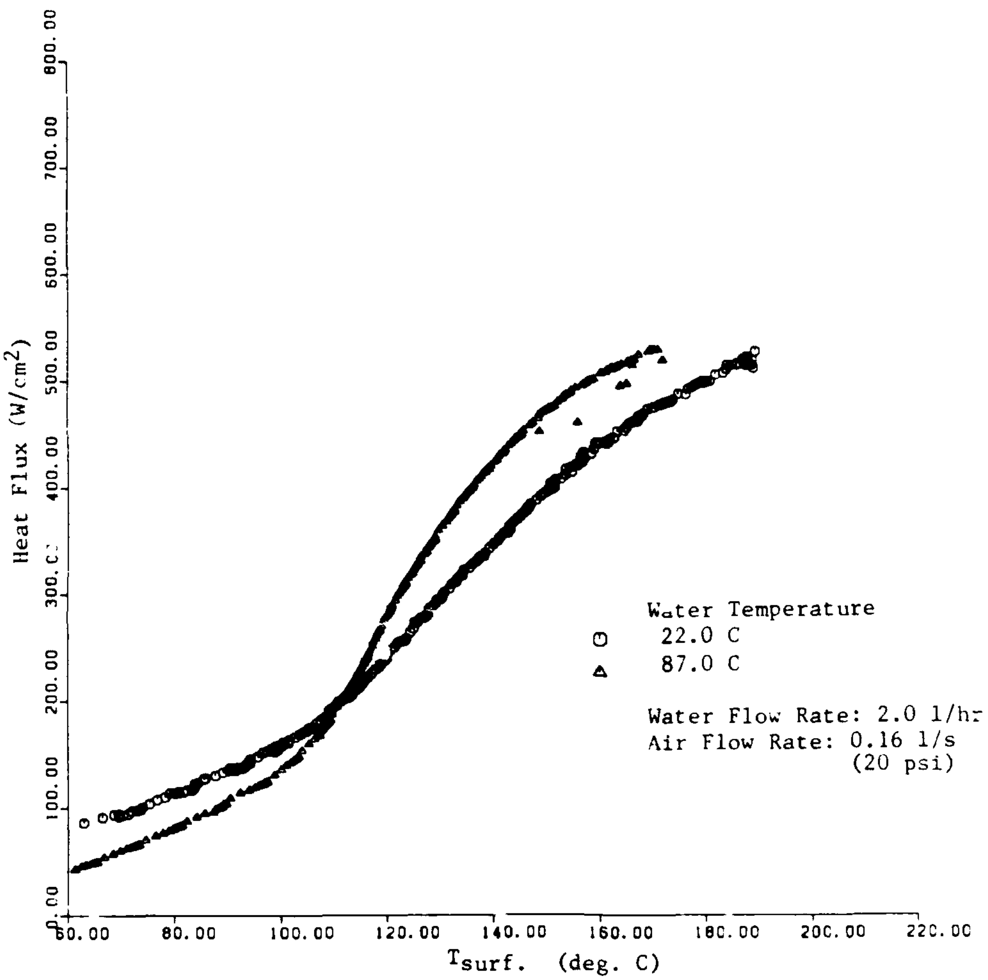

Figure 4.7 Effect of Coolant Temperature - 2

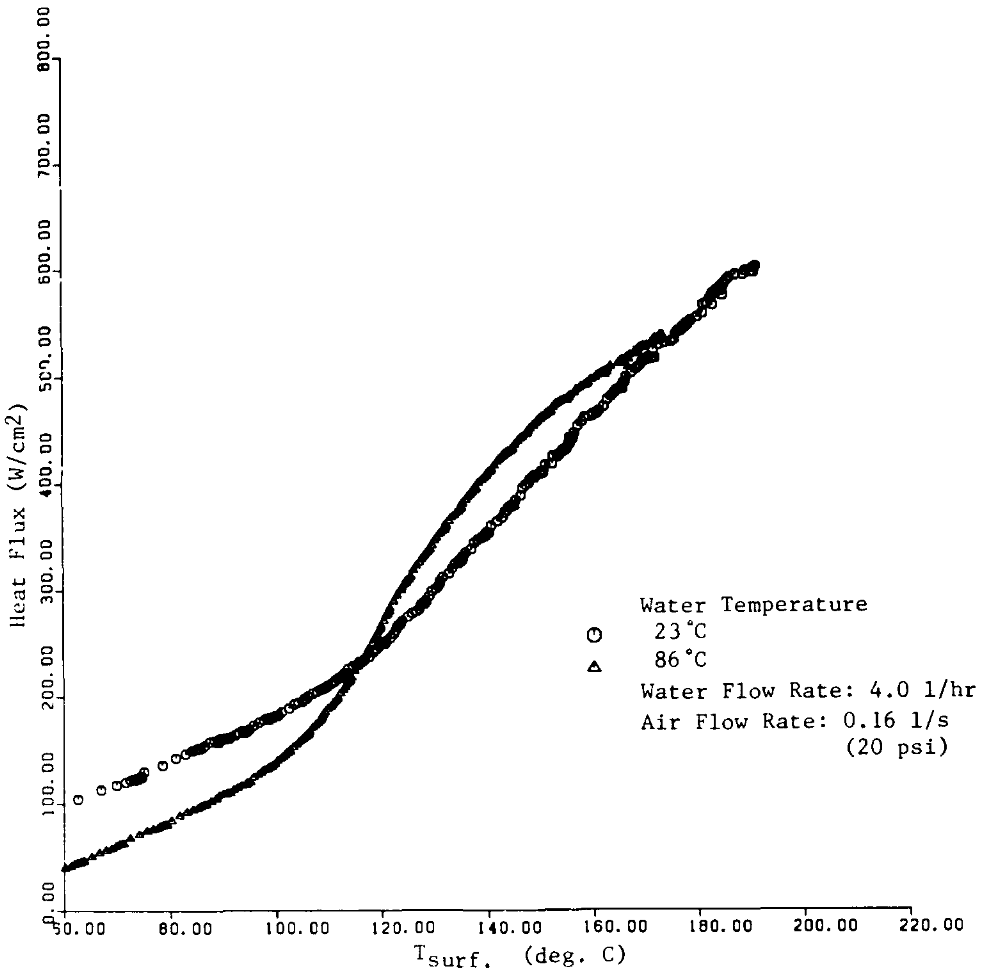

Figure 4.8 Effect of Coolant Temperature - 3

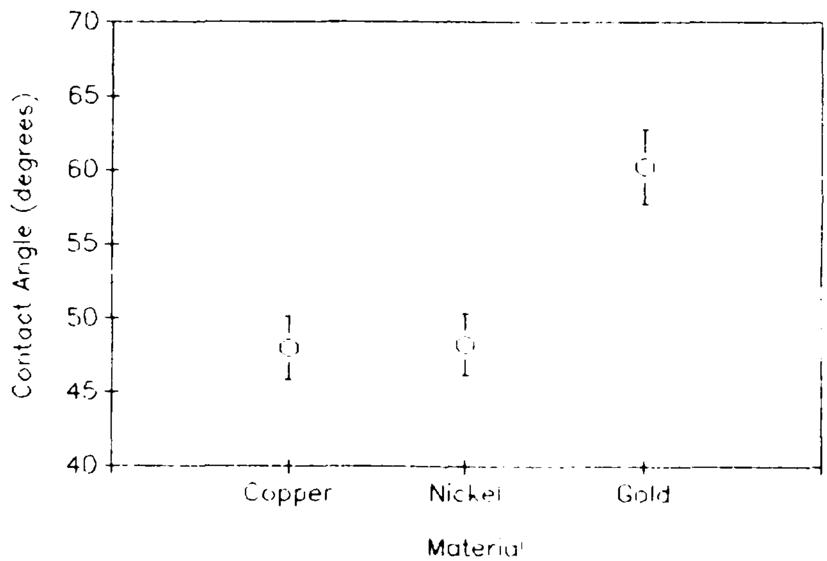

Figure 4.9 Contact Angles

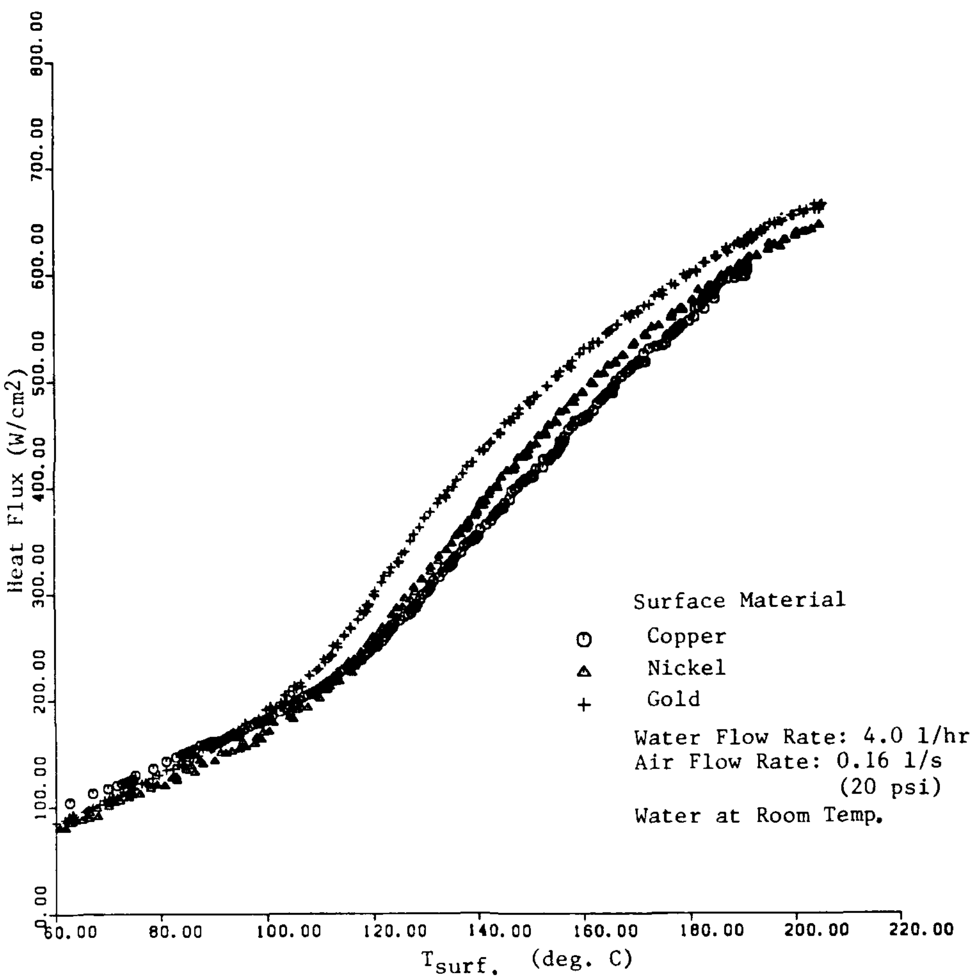

Figure 4.10 Effect of Surface Contact Angle - 1

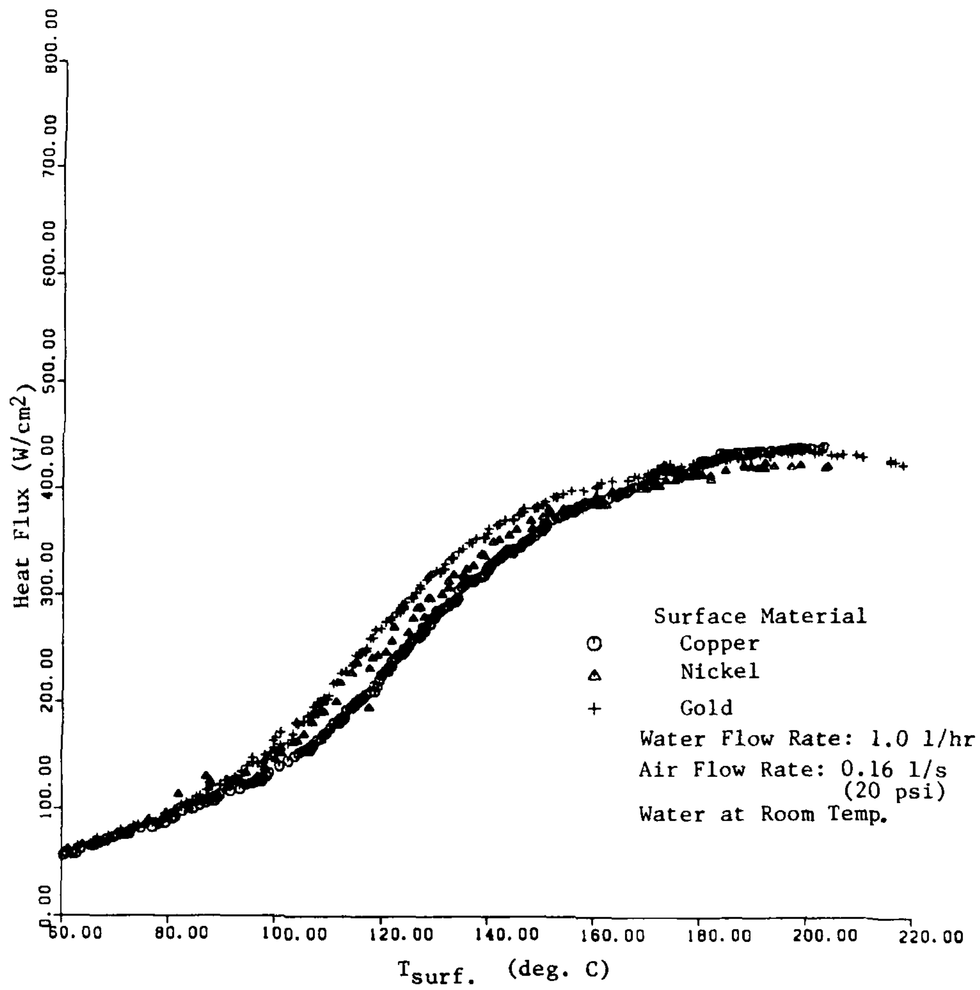

Figure 4.11 Effect of Surface Contact Angle - 2

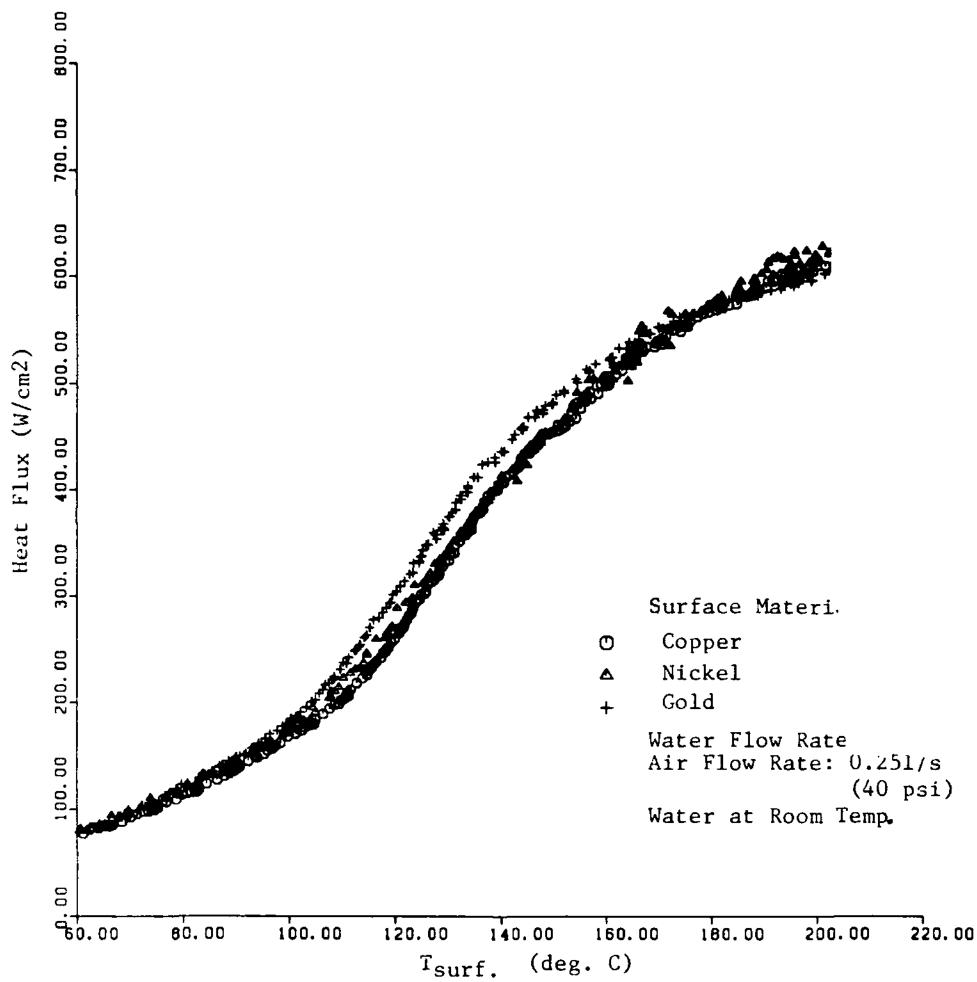

Figure 4.12 Effect of Surface Contact Angle - 3

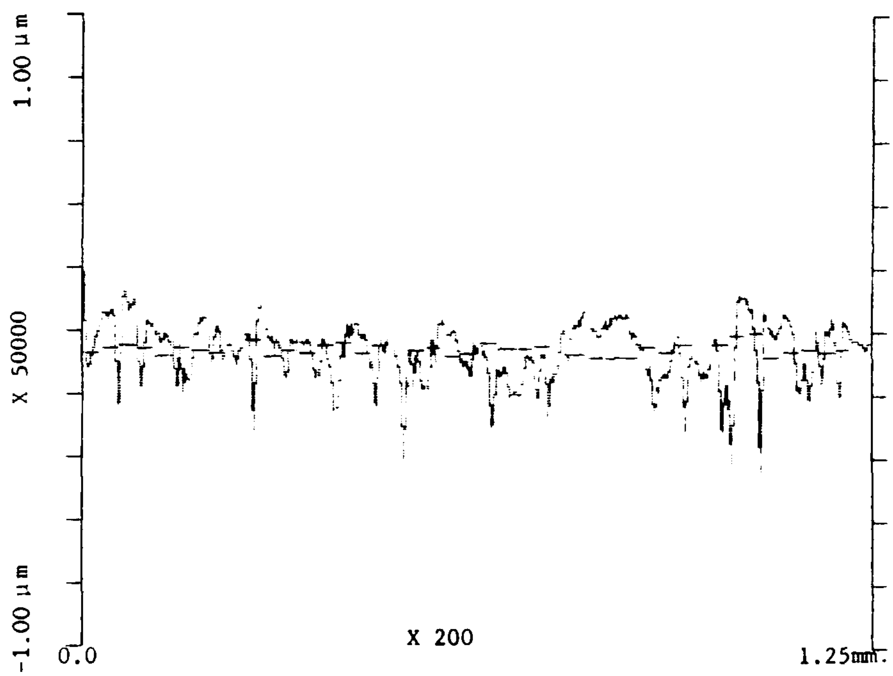

Figure 4.13 Roughness Profile - 14 μm grit polish

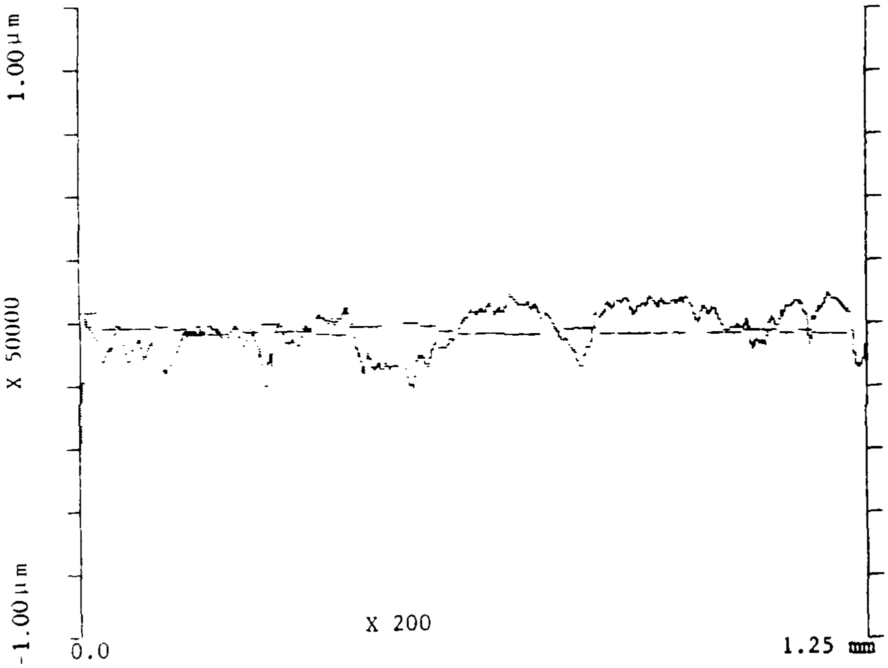

Figure 4.14 Roughness Profile - 0.3 μm grit polish

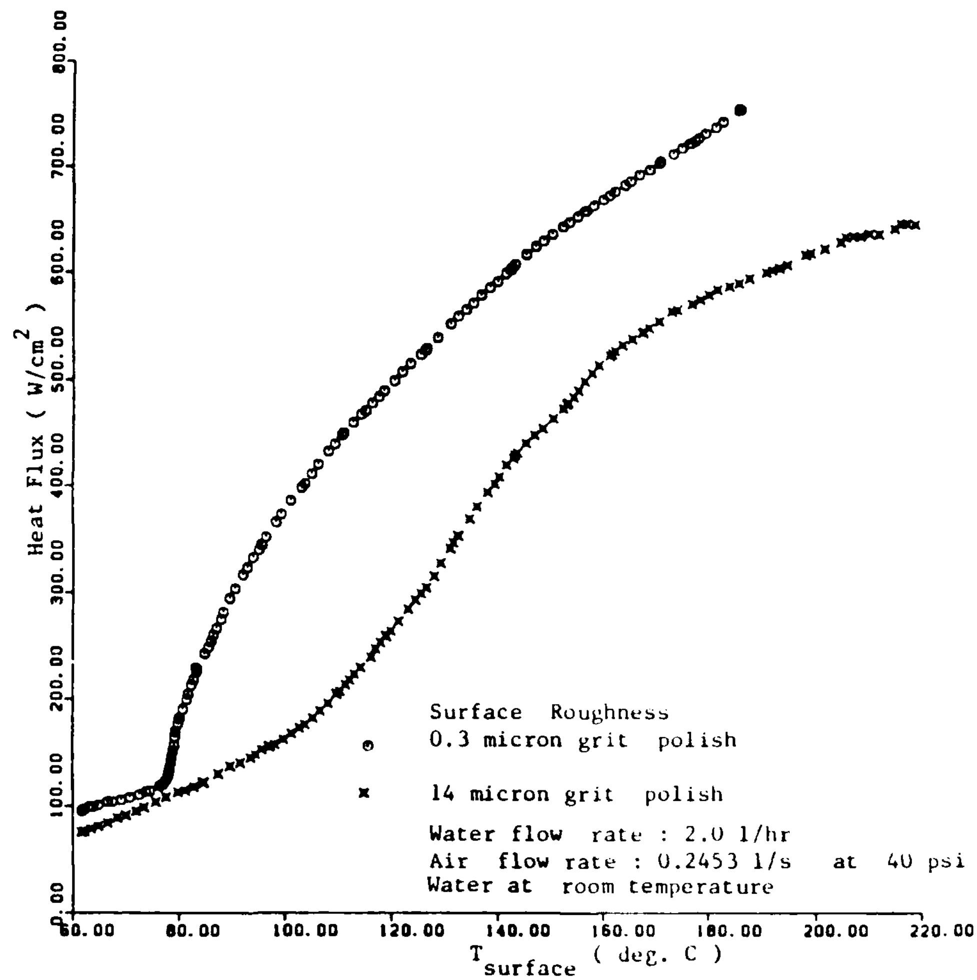

Figure 4.15 Effect of Surface Roughness - 1

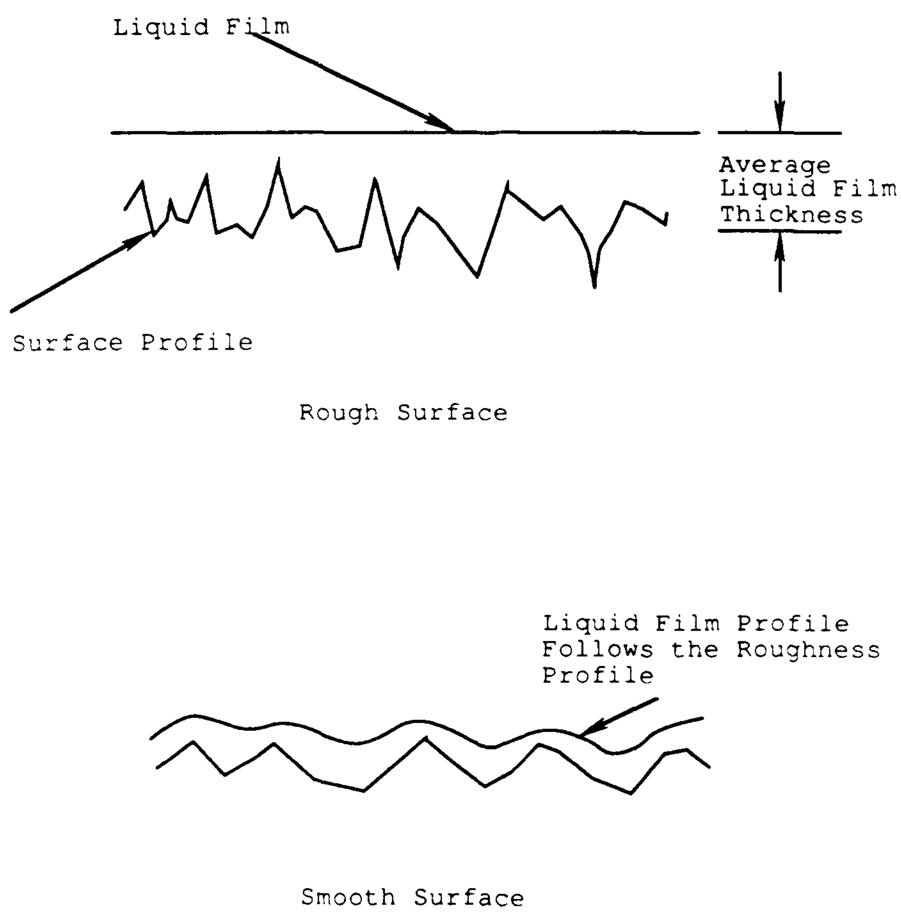

Figure 4.16 Film Thickness

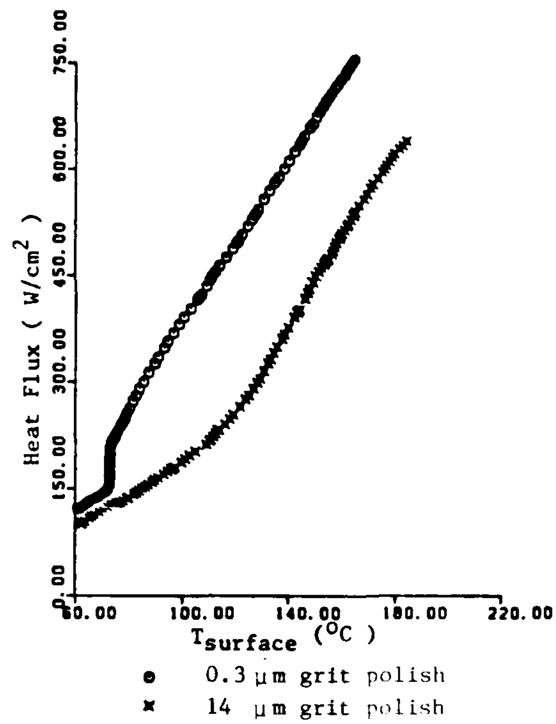

Water flow rate: 4.0 l/hr
Air flow rate: 0.25 l/s (40 psi)
Water at room temperature

Figure 4.17 Effect of Surface Roughness - 2

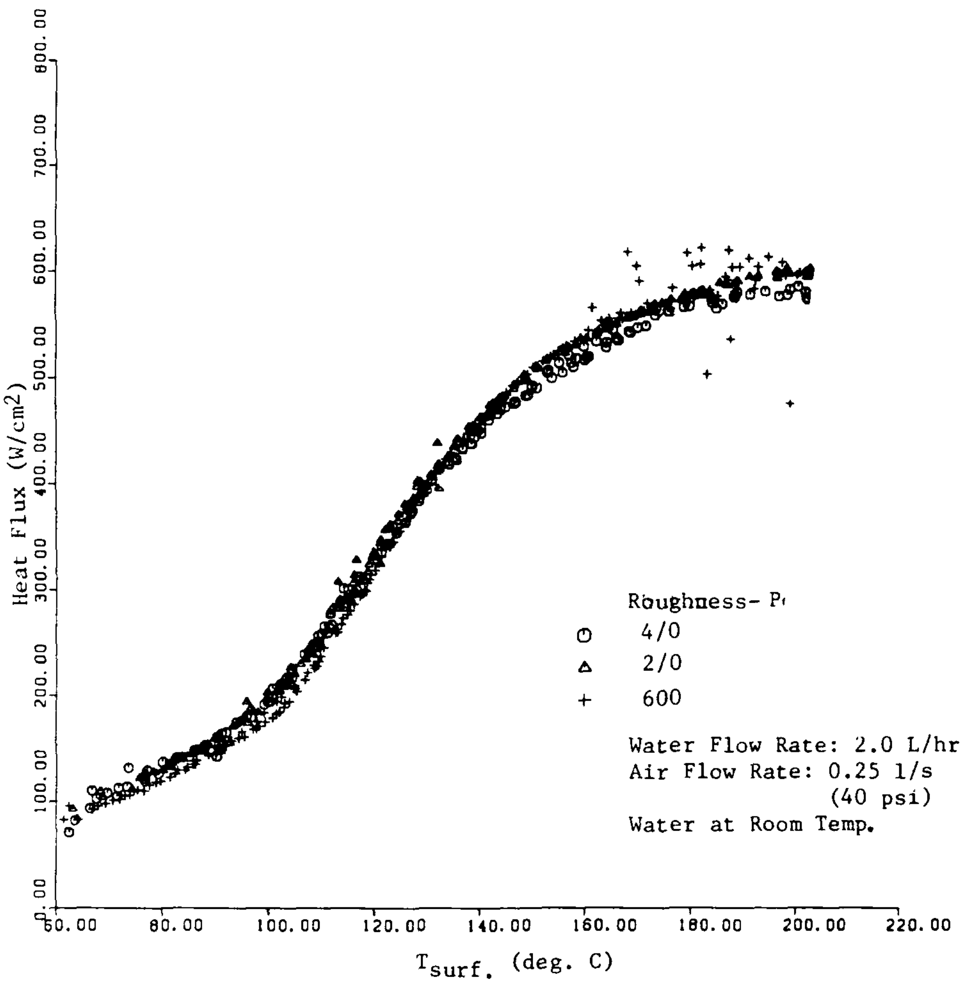

Figure 4.18 Effect of Surface Roughness - 3

Table 3.1 Thermocouple Calibration Constants

Polynomial Coefficients	Copper-Constantan	Copper-Silver	Constantan-Silver
a_0	7.2633364E-07	-8.2093389E-06	-5.3587533E-06
a_1	3.8522987E-05	1.5605573E-06	4.0999952E-05
a_2	4.3124505E-08	-1.0782581E-08	-5.3762608E-08
a_3	2.2868553E-11	1.8549296E-10	9.1690699E-10
a_4	-4.4466612E-13	-1.4160927E-12	-4.7932901E-12
a_5	1.7744421E-15	5.7250733E-15	1.4669923E-14
a_6	-3.3649500E-18	-1.1647572E-17	-2.5512934E-17
a_7	2.4993808E-21	9.3373451E-21	1.8473597E-20

Table 4.1 Roughness Parameters

Surface Material	Roughness Parameters	
	R_p μm	R_q μm
Copper	0.20	0.08
Nickel	0.20	0.08
Gold	0.20	0.11

☆ U.S. GOVERNMENT PRINTING OFFICE